Secondary reactions of aromatics-derived oxygenated organic molecules lead to plentiful highly oxygenated organic molecules within an intraday OH exposure

Yuwei Wang[1], Chuang Li[1], Ying Zhang[1], Yueyang Li[1], Gan Yang[1], Xueyan Yang[1], Yizhen Wu[1], ~~Chuang Li[1]~~, Lei Yao[1,2], Hefeng, Zhang[3*], Lin Wang[1,2,4,5,6] *

[1] Shanghai Key Laboratory of Atmospheric Particle Pollution and Prevention (LAP³), Department of Environmental Science and Engineering, Jiangwan Campus, Fudan University, Shanghai 200438, China

[2] Shanghai Institute of Pollution Control and Ecological Security, Shanghai 200092, China

[3] State Environmental Protection Key Laboratory of Vehicle Emission Control and Simulation, Vehicle Emission Control Center of Ministry of Ecology and Environment, Chinese Research Academy of Environmental Sciences, Beijing 100012, China

[4] IRDR International Center of Excellence on Risk Interconnectivity and Governance on Weather/Climate Extremes Impact and Public Health, Fudan University

[5] National Observations and Research Station for Wetland Ecosystems of the Yangtze Estuary, Shanghai, China

[6] Collaborative Innovation Center of Climate Change, Nanjing, 210023, China

Corresponding Author: H.Z., email, zhanghf@craes.org.cn; phone, +86-10-84915586

L.W., email, lin_wang@fudan.edu.cn; phone, +86-21-31243568

ABSTRACT. Highly oxygenated organic molecules (HOMs) can participate in new particle formation (NPF) and enhance growth of newly formed particles partially because of their low volatility. Previous studies have shown formation of HOMs via autoxidation reactions of RO_2 intermediates generated by OH-initiated oxidation of anthropogenic volatile organic compounds (VOCs). It was also suggested that multi-generation OH oxidation could be an important source for aromatics-derived HOMs. However, our understanding on the generation of aromatics-derived HOMs are still insufficient, especially for their formation mechanisms, which determine molar yields of HOMs and are essential to the establishment of global chemical box models related to HOMs. In this study, with a potential aerosol formation oxidation flow reactor (PAM OFR), ~~a~~two series of OH-initiated oxidation experiments of 1,3,5-trimethylbenzene (1,3,5-TMB) were conducted to investigate ~~the influences of the extent of OH exposure on~~ the formation of aromatics-derived HOMs. In the first series, ~~The~~the evolution of oxidation products of 1,3,5-TMB in an OH exposure range of $(0.5 – 5.0)\times10^{10}$ molecules cm^{-3} s, equivalent to an OH exposure of $0.7 – 6.9$ hours at an OH concentration ([OH]) of 2×10^6 molecules cm^{-3}, was investigated by a nitrate-based chemical ionization mass spectrometer and a Vocus proton-transfer-reaction mass spectrometer, indicating significant secondary OH

37 chemistry during the ageing of stabilized first generation oxygenated products within an
38 intraday OH exposure and formation of various HOMs with lower double bond equivalence
39 (DBE)more oxygen content and thus lower volatility. In addition, organonitrates, formed after
40 the introduction of NO_x into the reaction systems, further confirmed the existence of such
41 secondary reactions. The second series of experiments was conducted with same residence time
42 but much lower [OH], which also shows the generation of multi-generation HOMs with an [OH]
43 as low as 1.06×10^7 molecules cm^{-3} for 53 s, i.e., an OH exposure of around 5.86×10^8 molecules
44 cm^{-3} s. Our study suggests an important role of secondary OH chemistry in the oxidation of
45 aromatics, if these oxygenated products survived long enough in the ambient, and elucidates
46 detailed formation mechanisms of certain HOM products.

1 Introduction

48   OH radicals can react with volatile organic compounds (VOCs) in the atmosphere,
49 converting primary pollutants to secondary ones. Generated from oxidation of VOCs,
50 oxygenated organic molecules (OOMs) are crucial in a variety of atmospheric chemical
51 processes, contributing efficiently to the formation of secondary organic aerosols (SOAs) and
52 ground-level O_3 (Ng et al., 2010; Wang et al., 2022; Qu et al., 2021). Among the enormous
53 number of oxygenated VOCs (OVOCs), highly oxygenated organic molecules (HOMs) have
54 recently attracted significant attention (Bianchi et al., 2019). Most of HOMs are low volatile
55 volatility organic compounds (LVOCs) or extremely low volatile volatility organic compounds
56 (ELVOCs), and thus are able to drive the initial formation of nucleated particles under certain
57 conditions and contribute to the subsequent growth of newly-formed particles, which finally
58 enhance SOA formation (Tröstl et al., 2016; Lehtipalo et al., 2018; Stolzenburg et al., 2018;
59 Mohr et al., 2019; Qiao et al., 2021).
60   Formation of HOMs is typically triggered by oxidation of VOCs in the gas phase. Peroxy
61 radicals (RO_2) are generated at the initial step and will undergo an intramolecular hydrogen
62 atom shift forming a hydroperoxide functionality and an alkyl radical. A molecular oxygen will
63 rapidly attach to this alkyl radical and form a new and more oxidized RO_2. This reaction is
64 called as autoxidation and the newly formed RO_2 can go through another autoxidation or
65 bimolecular termination reactions to form a stabilized product (Crounse et al., 2013).
66 Autoxidation is suggested to be responsible for widely detected HOMs in the atmosphere,
67 because it can form highly oxygenated RO_2 in a short time scale. In terms of biomolecular
68 reactions, RO_2 reacts appreciable only with hydroperoxyl radical (HO_2), NO, and another RO_2.
69 The RO_2 reaction chain in polluted areas is largely terminated by NO, which prohibits
70 generation of compounds with high oxidation levels and reduces yields of HOMs (Bianchi et
71 al., 2019).

72   Nevertheless, autoxidation reactions alone are not enough to explain the large numbers of

73   oxygen atoms and low double bond equivalence (DBE, calculated as $nC - \frac{nH+nN}{2} + 1$ where

74   nC, nH, and nN stand for number of containing carbon, hydrogen, and nitrogen, respectively)

75   in HOMs observed in laboratory experiments and ambient campaigns. Take alkylbenzenes as

76   an example, previous studies suggest that the main products of OH-initiated oxidation of

77   alkylbenzenes (C_xH_{2x-6}, x=7, 8, or 9), i.e., bicyclic peroxy radicals (BPR, $C_xH_{2x-5}O_5\cdot$, x=7, 8, or

78   9) (Jenkin et al., 2003), can undergo an autoxidation reaction and form a new peroxy radical,

79        $C_xH_{2x-5}O_7\cdot$ (x=7, 8, or 9) (Wang et al., 2017).The autoxidation of BPR could be fast if it has a

80   favorable structure, as found in a previous study (Wang et al., 2017). On the other hand, the

81   structure of resulting $C_xH_{2x-5}O_7\cdot$ is strongly different from that of BPR, whose autoxidation

82   reaction rate can be as low as the order of 0.001 s^{-1}, since it lacks enhancements from favorable

83   transition state geometries and substitutes or resonance structures (Bianchi et al., 2019; Otkjær

84   et al., 2018). Such a slow autoxidation reaction rate cannot explain the extensive existence of

85   HOM monomers with more than 7 oxygen atoms and HOM dimers with more than 10 oxygen

86   atoms, which are the maximum numbers of oxygen atoms in stabilized monomer and dimer

87   products, respectively, formed from $C_xH_{2x-5}O_7\cdot$ (Molteni et al., 2018; Wang et al., 2020b;

88   Mentel et al., 2015). Another possibility is the formation of a second oxygen bridge after the

89   hydrogen shift of BPR (Molteni et al., 2018), but this reaction pathway would not allow a

90   further oxygenation reaction without a breakage of the carbon ring, which is also unpromising.

91   A very recent investigation offers new insights into the formation mechanism of these products,

92   indicating the molecular rearrangement of BPR can initiate a series of autoxidation (Iyer et al.,

93   2023). However, the formation mechanism of HOMs with a large hydrogen atom number, i.e.,

94   low DBE, is still vague. ~~e.g.,~~For example, monomer products with 16 hydrogen atoms in the

95   OH-initiated oxidation of TMB and with 14 hydrogen atoms in the OH-initiated oxidation of

96   xylene were observed in the laboratory, both with a DBE of 2 lower than their precursors'

97   (Molteni et al., 2018), but their formation mechanisms cannot be explained by any known

98   mechanisms with only one OH attack.

99   Multigeneration reactions of VOCs complicate HOMs' formation. Previous studies

100   indicate that HOMs can also be formed by sequential oxidation of stabilized first-generation

101   products of benzene and toluene (Garmash et al., 2020; Cheng et al., 2021). Garmash et al.

102   (2020) conducted OH oxidation experiments of benzene and toluene with an OH exposure

103   equivalent to atmospheric oxidation times of 10 hours – 15 days at OH concentrations of ~10^6

104   molecules cm^{-3}. Cheng et al. (2021) simulated oxidation of benzene and toluene with an OH

105   exposure equivalent to 2.4 – 19.4 days of atmospheric photochemical ageing. Certainly, such

106   extremely high OH exposures favor secondary OH chemistry and help to facilitate our

understanding on product distributions, but such a long timescale limits atmospheric implications of their results, given the complex physical and chemical processes at night.

Compared to benzene and toluene, trimethylbenzene (TMB) is a precursor characterized with much larger HOM molar yields when reacted with OH, and the abundance of TMB in the atmosphere is unignorable (Molteni et al., 2018; Yuan et al., 2012). Previous laboratory experiments on TMB-derived HOMs mainly focused on the autoxidation reactions of BPR and the influences of NO_x, while the quantity of experiments was finite ~~with a limited range of OH exposure~~, ~~bringing down the universality and applicability of conclusions~~restricting the application of their conclusions to the more atmospheric relevant condition (Tsiligiannis et al., 2019; Wang et al., 2020b). From the mechanism perspective, a number of HOM monomers with more than 7 oxygen atoms detected in the OH-initiated oxidation of TMB were previously assumed to be generated via multiple autoxidation reactions (Molteni et al., 2018). Nevertheless, a subsequent OH oxidation of the first-generation oxygenated products might be more plausible for the formation of HOM monomers with more than 7 oxygen atoms from the present point of view. Indeed, laboratory experiments show that RO_2 formed during the second-generation OH oxidation of the first-generation stabilized oxidation products can also undergo autoxidation reactions, which entangles reaction mechanisms potentially involved in the formation of those HOMs and justifies more investigations on the multigeneration OH oxidation of aromatics (Wang et al., 2020b). OH with an atmospheric concentration ([OH]) up to $6\times10^6 - 2.6\times10^7$ molecule cm^{-3}, which is several times higher than the typical average atmospheric ~~OH concentration~~ [OH], 1.5×10^6 molecule cm^{-3} (Jacob, 1999), has been frequently observed in both urban and suburban environments in China (Tan et al., 2019; Lu et al., 2012), leading to a realistic implication of multigeneration OH oxidation. Therefore, it is imperative to study chemical characteristics of formation reactions of HOMs at different OH exposures, especially those fewer than or equivalent to one day of atmospheric oxidation.

In this study, a series of laboratory experiments were conducted on the OH-initiated oxidation of 1,3,5-TMB, selected as an example of anthropogenic VOCs with [OH] as high as $9.32\times10^7 - 1.03\times10^9$ molecule cm^{-3} and an OH exposure equivalent to atmospheric oxidation times of roughly 0.7 – 6.9 hours at an average daytime [OH] of 2.0×10^6 molecules cm^{-3}. A nitrate-based chemical ionization mass spectrometer (nitrate CIMS) and a Vocus proton-transfer-reaction mass spectrometer (Vocus PTR) were deployed to measure the oxidation products and the precursor, respectively. From the evolution of oxygenated products, we explored secondary OH chemistry of stabilized first-generation oxygenated products generated by the oxidation of 1,3,5-TMB. Furthermore, the influence of NO on the formation of HOMs was investigated by introducing N_2O into the reaction system via formation of organonitrates.

142 In addition, another series of experiments under atmospheric relevant [OH] were conducted to

143 confirm the applicability of the above-developed multi-generation OH oxidation mechanisms

144 in the ambient atmosphere.

2 Methods

146 OH-initiated oxidation of 1,3,5-TMB was investigated in a potential aerosol formation

147 oxidation flow reactor (PAM OFR) system at $T = 298 \pm 1$ K and a pressure of 1 atm (Lambe et

148 al., 2015). Two series of experiments were conducted, one under high [OH] conditions and the

149 other under low [OH] conditions. Hereafter, we refer to the series of high [OH] experiments as

150 'the 1st-round experiments' and the low [OH] as 'the 2nd-round experiments', respectively. The

151 i^{th} experiment in the 1st-round experiments is labelled as 1-i and the one in the 2nd-round

152 experiments as 2-i, where i stands for its serial number. The experimental settings in this study

153 differed slightly from what were used previously (Wang et al., 2020b). In the 1st-round

154 experiments, Fforty OH experiments without NO$_x$ (Exp. 1-1 – 1-40) and twenty-eight NO$_x$

155 experiments with NO$_x$ (Exp. 1-41 – 1-68) were performed,. Seven experiments were conducted

156 in the 2nd-round, four without NO$_x$ and three with NO$_x$. the The experimental conditions of

157 which are summarized in Table S1, including concentrations of the precursor, ozone, and NO

158 and NO$_2$. The equivalent OH exposure in the OFR for each experiment was estimated according

159 to the precursor consumption, also listed in Table S1. OH exposures in the OFR were in the

160 range of ($0.5$2 – $5.0$48.7)$\times 10^{10}$-10^9 and $(0.6 – 5.5) \times 10^9$ molecules cm^{-3} s in the 1st-round and

161 2nd-round experiments, respectively. equivalent to atmospheric oxidation times of roughly 0.7

162 – 6.9 hours for 1,3,5-TMB at an average daytime OH radical concentration of 2.0×10^6

163 molecules cm^{-3}. In contrast, the OH oxidation lifetime for 1,3,5-TMB is around 2.4 hours at the

164 aforementioned atmospheric average daytime OH concentrations.

165 A home-made 1,3,5-TMB/N$_2$ cylinder was used as a stable gaseous precursor source in the

166 experiments, from which the flow rate of 1,3,5-TMB/N$_2$ varied between 1 – 3 sccm (standard

167 cubic centimeter per minute, standard to 0 °C, 1 atm), leading to 28.9 – 62.7 ppb of 1,3,5-TMB

168 in the OH oxidation 1st-round experiments, and 30.8 or 34.5 ppb of 1,3,5-TMB in the 2nd-round

169 experiments, respectively (Table S1). A total flow of 15 slpm (standard liters per minute,

170 standard to 0 °C, 1 atm) zero-gas generated by a zero-gas generator (model 737-13, Aadco

171 Instruments Inc.), together with the 1,3,5-TMB/N$_2$ flow, was introduced into the OFR. The

172 reaction time in this both series of experiments was kept at around 53 s. and the flow reactor

173 was kept as a plug flow in both series. The flow in the PAM OFR is laminar with a very low

174 axial mixing, as characterized with a Taylor dispersion model in a previous study (Lambe et al.,

175 2011). Among the 15 slpm zero-gas, 6 slpm was initially passed through a Nafion humidifier

(Perma Pure Model FC100-80-6MSS) filled with ultra-pure water and finally converged with the main flow into the OFR to achieve and keep a desired RH of 20.0 ± 2.5 % in the OFR throughout all the experiments, and 2 slpm was initially passed through a separate ozone chamber, resulting in an initial ozone concentration of around 429 – 881 ppb in the OFR in the 1st-round experiments and 123 – 152 ppb in the 2nd-round experiments, respectively. The OFR was operated with only the 254 nm lights on, under which the primary oxidant production reactions in the OFR were $O_3 + hv\,(254\,nm) \rightarrow O_2 + O(^1D)$ and $O(^1D) + H_2O \rightarrow 2OH$. After turning on of UV lights, a certain HOM compound is believed to be generated if its signal is more than 3 standard deviations of its background signal. If the fluctuations in the 1-min-averaged signals of both TMB in the Vocus PTR and typical HOMs (i.e., $C_9H_{14}O_7(NO_3)^-$) in the nitrate CIMS are within 2% during a 10-min period, we assume that a steady state has been reached. It usually took around no more than 2 minutes for the signals of HOMs to stabilize after the adjustment of UV lights. We typically monitored the reaction products for around 20 minutes for each experiment. An ozone monitor (Model 106-M, 2B technologies) and a trace-gas analyzer for NO-NO₂-NOₓ (Thermo, 42i-TL) were placed at the exit of the OFR to measure concentrations of ozone and NOₓ, respectively.

Non-tropospheric VOC and OVOC photolysis is a typical issue that should be taken into account when evaluating the settings of OFR laboratory experiments, especially under the high UV light dose settings in the 1st-round experiments. Photolysis of the precursor and HOMs were evaluated, showing that photolysis was not a contributor to our observation. The photolysis rate of 1,3,5-TMB can be estimated based on the absorption cross-sections of 1,3,5-TMB at 254 nm (Keller-Rudek et al., 2013) and UV photon fluxes estimated by a chemistry model discussed in the following sections. The ratio of photolysis-to-OH reaction in our 1st-round experiments was merely 0.010 – 0.033. Hence, photolysis of 1,3,5-TMB was insignificant in the OFR. For stabilized products such as C9 and C18 HOMs, the cross sections of organic molecules are usually ~ 3.9×10^{-18} - 3.9×10^{-17} cm² (Peng et al., 2016), while the reaction rate between OH and the stabilized first-generation products are estimated to be around 1.28×10^{-10} molecule⁻¹ cm³ s⁻¹, as suggested by MCM (Jenkin et al., 2003). Hence, the ratio of photolysis rates of C9 and C18 HOMs to their secondary OH oxidation rates is estimated to be merely around 0.020 – 0.056 in the 1st-round experiments. In the 2nd-round, the influences of photolysis should be even lower due to the much lower light intensity.

For experiments with NOₓ in the 1st-round experiments, 350 sccm N₂O (99.999%, Air Liquid) was added into the OFR to produce and sustain NOₓ mixing ratios at levels that were sufficiently high to be a competitive sink for RO₂ radicals. NO and NO₂ were produced via the reaction $N_2O + O(^1D) \rightarrow 2NO$, followed by the reaction $NO + O_3 \rightarrow NO_2 + O_2$. Two sets of

211   irradiance intensities were chosen for NO_x experiments, generally resulting in two NO_x levels,

212   1.8 ppb NO + 70 ppb NO_2 (Exp. 1-41 – 1-54) and 4.8 ppb NO + 120 ppb NO_2 (Exp. 1-55 – 1-

213   68) at the exit of the OFR. With the aim to slightly modify OH exposure but keep NO_x

214   concentrations constant among each set of experiments, the initial concentrations of 1,3,5-TMB

215   were adjusted in a large range (16.7 – 84.1 ppb), as an increase in the precursor concentration

216   corresponds to a larger sink for OH, while RH and irradiances were not changed. In the 2nd-

217   round experiments, due to the lower (O^1D) in the PAM OFR, 2.5 slpm pure N_2O was utilized

218   instead, whereas the total flow rate was kept the same as that in the 1st-round. We lowered the

219   light intensity to obtain lesslower [OH] in the PAM OFR, which also resulted in fluctuations in

220   the NO concentrations ([NO]) from 1.3 to 7.1 ppb and the NO_2 concentrations ([NO_2]) from 11

221   to 38 ppb.

222   A nitrate CIMS (Ehn et al., 2014; Eisele and Tanner, 1993) and a Vocus PTR (Krechmer

223   et al., 2018) were deployed at the exit of the OFR to measure the oxidation products of 1,3,5-

224   TMB in the 1st-round experiments. These two mass spectrometers have been well characterized

225   in a previous study (Wang et al., 2020b).

226   In this study, tThe sample flow rate for the nitrate CIMS in the 1st round-experiments was

227   8 slpm through a Teflon tube with an outer diameter (OD) of 1/4 in. and a length of 70 cm. The

228   sheath flow for the nitrate CIMS was supplied by a zero-gas generator at a flow rate of 15 slpm.

229   Mass resolution was approximately 8000 for ions with m/z larger than 200 Th. HOMs generated

230   from TMB oxidation were charged in the ambient pressure interface region by collisions with

231   nitrate clusters, $(HNO_3)_x \cdot NO_3^-$ ($x = 0 – 2$), and detected by nitrate CIMS as clusters with NO_3^-,

232   i.e., $HOM \cdot NO_3^-$ (Hyttinen et al., 2015). In addition, HOMs' signals were corrected with relative

233   transmission efficiencies of our nitrate CIMS obtained via a method reported previously

234   (Heinritzi et al., 2016). We followed the same sampling method of PAM OFR as those in

235   previous studies, in order to obtain a similar flow tube residence time distributions (RTDs) and

236   thus validate usage of a modified PAM_chem_v8 model to estimate concentrations of radicals

237   in the OFR as discussed below. We acknowledge that this is not a perfect sampling setting for

238   nitrate CIMS. However, the reduction in the sampling efficiencies of various HOMs is likely

239   to be close, if not identical, which keeps the distributions of HOMs.

240   Vocus PTR was applied to quantify precursor concentrations and measure volatile and

241   intermediate volatility oxidation products. The focusing ion-molecule reactor (FIMR) was

242   heated up and its temperature was maintained at 100 ℃ during the experiments. The FIMR can

243   be operated under 2.0 mbar without a strong interference from corresponding water clusters

244   when ionizing the neutral compounds. The Vocus front and back voltages were 650 V and 15

245   V, respectively, forming an axial voltage of 635V and a reduced electrical field (*E/N*, where E

246 is the electric field strength and N is the number density of the buffer gas in FIMR) of 180 Td.

247 The radio frequency (RF) voltages and frequency were set to be 450 V and 1.3 MHz,

248 respectively. The sample flow was introduced to the Vocus PTR through a Teflon tube with an

249 OD of 1/4 in. and a length of 120 cm from the OFR. A total sample flow of 1.4 slpm was

250 maintained by a pump with an orifice to minimize the delay time of sampling, from which

251 approximately 125 sccm was sampled into the FIMR through a capillary tube.

252 In the 2nd-round experiments, , a Vocus CI-TOF (Towerk AG, Switzerland) equipped with

253 a Vocus Aim inlet and the same nitrate-ion chemical ionization source as adopted in the 1st-

254 round experiments was utilized to measure oxidation products, hereafter referred as nitrate CI-

255 TOF. The nitrate CI-TOF was characterized with a flat transmission efficiency between m/z 60

256 Th and m/z 500 Th, as well as a mass resolution of 10000 at m/z 200 Th.

257 In this series of experiments, the reaction products were sampled from the PAM OFR via

258 a 30 cm-long Teflon tube with a 1/2 in. OD to our nitrate CI-TOF. The Vocus PTR and the

259 ozone monitor were connected to the PAM OFR from a separate port via a 120 cm-long Teflon

260 tube with a 1/4 in. OD.

261 We did not quantify HOMs' concentrations. Since the inner diameters of PAM OFR,

262 sampling tube, and the nitrate CIMS inlet were different, and two reducing unions were used

263 during sampling, the estimation of the penetration efficiency and sampling efficiency of HOMs

264 are of a significant uncertainty. The initial concentrations of TMB utilized in the both sets of

265 experiments fluctuated slightly, which resulted from sample preparation processes, but

266 generally were around 50 ppbv. and were more obvious in the 1st-round experiments. Therefore,

267 in the discussion on the data of the 1st-round experiments, we tried to minimize potential

268 influences of the differences in the initial TMB concentrations on the signals of HOMs by

269 normalizing the HOMs signals with the initial TMB signal. To precisely illustrate changes in

270 the abundance of HOMs at different OH exposures, a normalized signal was chosen to present

271 the abundance of detected HOMs, which is defined as the ratio of the signals of HOMs in the

272 nitrate CIMS normalized by the reagent ions and the initial signal of 1,3,5-TMB, i.e.,

273 $S(HOMs)/S(TMB)$. $S(HOMs)$ is the signal of HOM detected by the nitrate CIMS normalized

274 with the signal of reagent ions, whereas $S(TMB)$ is the initial signal of 1,3,5-TMB detected by

275 the Vocus PTR.

276 To validate our settingscompare chemical regimes of the two series of experiments and the

277 ambient atmosphere, a PAM chemistry model (PAM_chem_v8), utilized widely in previous

278 studies, were chosen with the latest updates to calculate radical profiles in our OFR (Li et al.,

279 2015; Cheng et al., 2021; Wang et al., 2020b; Mehra et al., 2020; Lambe et al., 2015, 2018;

280 Peng and Jimenez, 2020; Lambe et al., 2017). This model is based on a photochemical box

281 model that includes chemistry of photolysis of oxygen, water vapor, and other trace gases by

282 the primary wavelengths of mercury lamps, and simplified VOC and RO_2 chemistry (Table S2),

283 but further reactions of the first-generation stabilized products and the second-generation

284 organic radicals are not considered. The detailed reactions involved with RO_2 include:

285 $$RO_2 + R'O_2 \rightarrow RO + R'O + O_2 \qquad (R1)$$

286 $$RO_2 + R'O_2 \rightarrow R = O + R'OH + O_2 \qquad (R2)$$

287 $$RO_2 + R'O_2 \rightarrow ROH + R' = O + O_2 \qquad (R3)$$

288 $$RO_2 + R'O_2 \rightarrow ROOR' + O_2 \qquad (R4)$$

289 $$RO_2 + HO_2 \rightarrow ROOH + O_2 \qquad (R5)$$

290 $$RO_2 + OH \rightarrow Products \qquad (R6)$$

291 $$RO_2 \xrightarrow{isomerization} Products \qquad (R7)$$

292 $$RO_2 + NO \rightarrow RO + NO_2 \qquad (R8)$$

293 $$RO_2 + NO \rightarrow RONO_2 \qquad (R9)$$

294 $$RO_2 \rightarrow physical\ loss \qquad (R10)$$
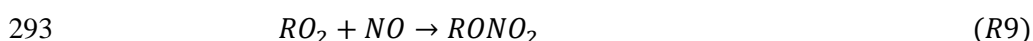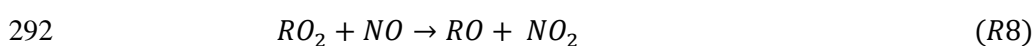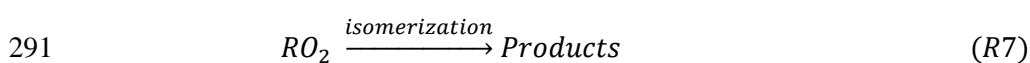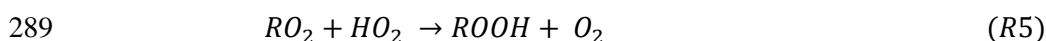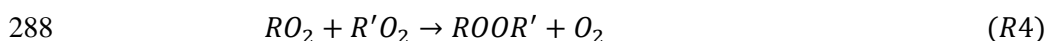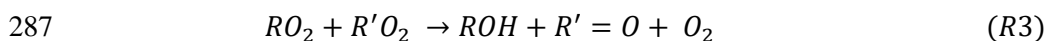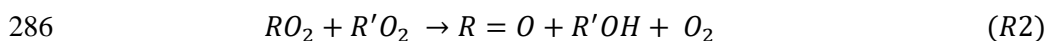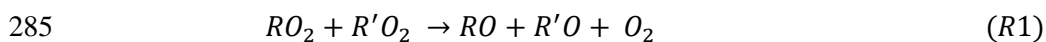
295 $R1$, $R2$, and $R3$ are reactions of $RO_2 + RO_2$, forming alkoxy radicals, carbonyl termination

296 products, and hydroxyl termination products, respectively. $R4$ is the accretion reaction,

297 forming dimers via combination of two monomeric RO_2. $R5$ is the reaction between RO_2 and

298 HO_2, forming hydroperoxyl radicals. $R6$ is the reaction between OH and RO_2, whose reaction

299 channels/products are proposed according to previous studies (Table S3). $R7$ is the

300 unimolecular reactions of RO_2 in the PAM OFR, among which the autoxidation reaction rate is

301 the most significant. $R8$ and $R9$ are the reactions between NO and RO_2, generating alkoxy

302 radicals and organonitrates, respectively. $R10$ is the physical loss of RO_2.

303 Kinetic data in the modified PAM_chem_v8 are obtained from the IUPAC (International

304 Union of Pure and Applied Chemistry) dataset (https://iupac-aeris.ipsl.fr, last access: 26

305 October 2023) and the MCM dataset (MCM v3.3.1, https://mcm.york.ac.uk/MCM/, last access:

306 9 October 2023), except for those that are specifically discussed in details in the supplement.

307 Note that the total RO_2 concentration is simplified to be the sum of concentrations of BPR and

308 $C_9H_{13}O_7\cdot$. In this work, the autoxidation reaction and the accretion reaction of 1,3,5-TMB-

309 derived BPR, as well as the subsequent reactions of the autoxidation product of BPR, i.e.,

310 $C_9H_{13}O_7\cdot$, are newly implemented or modified in this model (Reaction No. ~~41~~ 46 – ~~57~~ 62 in

311 Table S2). The newly implemented or modified reactions in this model are discussed in

312 Supplementary Text S1. NO_x-related reactions are also included in the model. When we

313 simulate experiments without NO_x, these reactions do not contribute to the simulation results.

314 For the 1st-round experiments, ~~T~~the input parameters of temperature, mean residence time,

315 water vapor concentration, O_3 concentration, and the initial 1,3,5-TMB concentration are 25 °C,

316 53 s, 0.~~8~~63%, 500 ppbv, and 50 ppbv, respectively, as measured directly ~~in the experiments~~.

317 For the 2nd-round experiments, the input parameters of O_3 concentration and the initial 1,3,5-

318 TMB concentration were updated as 150 ppbv and 30.8 ppbv, respectively. In the NO_x

319 experiments, the input flow rate of N_2O is 350 sccm in the 1st-round experiments and 2.5 slpm

320 in the 2nd-round experiments, respectively. The actinic flux at 254 nm, I_{254}, is constrained by

321 comparing OH exposures by model output and OH exposures estimated by the consumption of

322 1,3,5-TMB as measured by a Vocus PTR. Consumption of O_3 estimated by the model agrees

323 well with the measured results, with discrepancies being always within 10% at different OH

324 exposures.

325

326 **3 Results and discussion**

327 **3.1 ~~Validation of experiment settings~~Comparison of chemical regimes**

328   Concentration profiles of OH, RO_2, and HO_2 as a function of OH exposures in our high

329 [OH] experiments without NO_x, i.e., the 1st-round experiments, are illustrated in Figure S1a.

330 According to the modified PAM_chem_v8, when [OH] increased from ~~1.09~~9.32×~~10^8~~10^7 to

331 1.~~57~~03×10^9 molecule cm^{-3}, [HO_2] increased from ~~7.72~~7.25×10^8 to ~~3.18~~2.79×10^9 molecule cm$^-$

332 ^{3}, whereas [RO_2] concentrations increased from ~~4.83~~5.17×10^9 to ~~8.48~~9.5×10^9 molecule cm^{-3}.

333 The radical concentrations in high [OH] experiments with NO_x (Figure S1b) varied in a similar

334 range, with [RO_2] ranging from ~~3.89~~4.38×10^9 to ~~9.34~~9.13×10^9 molecule cm^{-3}, HO_2 ranging

335 from ~~3.66~~4.47×10^9 to ~~6.82~~6.47×10^9 molecule cm^{-3}, and OH ranging from ~~4.83~~3.86×10^8 to

336 ~~9.05~~7.82×10^8 molecule cm^{-3}, respectively. The ratios between HO_2/OH and RO_2/OH in ~~our~~ the

337 1st-round experiments were generally in the same order of magnitude with the ambient

338 atmosphere (Whalley et al., 2021). ~~are displayed in Figure S1c. The HO2/OH ratio ranged~~

339 ~~between 1.9 and 7.1 in our PAM OFR experiments without NOx, and the RO2/OH ratio ranged~~

340 ~~between 4.9 and 47.9. In experiments with NOx, the HO2/OH ratio ranged between 3.7 and 17.9,~~

341 ~~whilst the RO2/OH ratio ranged between 4.0 and 13.2. A recent comprehensive ambient~~

342 ~~campaign conducted in the wintertime central Beijing reported mean daytime peak~~

343 ~~concentrations of 8.8×10^7, 3.9×10^7, and 2.7×10^6 molecule cm^-3 for total RO2, HO2, and OH,~~

344 ~~respectively (Slater et al., 2020), which corresponds to ambient RO2/OH and HO2/OH ratios of~~

345 ~~32.6 and 14.4 (Figure S1c), respectively. Therefore, radical ratios in our flow tube were~~

346 ~~generally in the same order of magnitude with the ambient conditions.~~
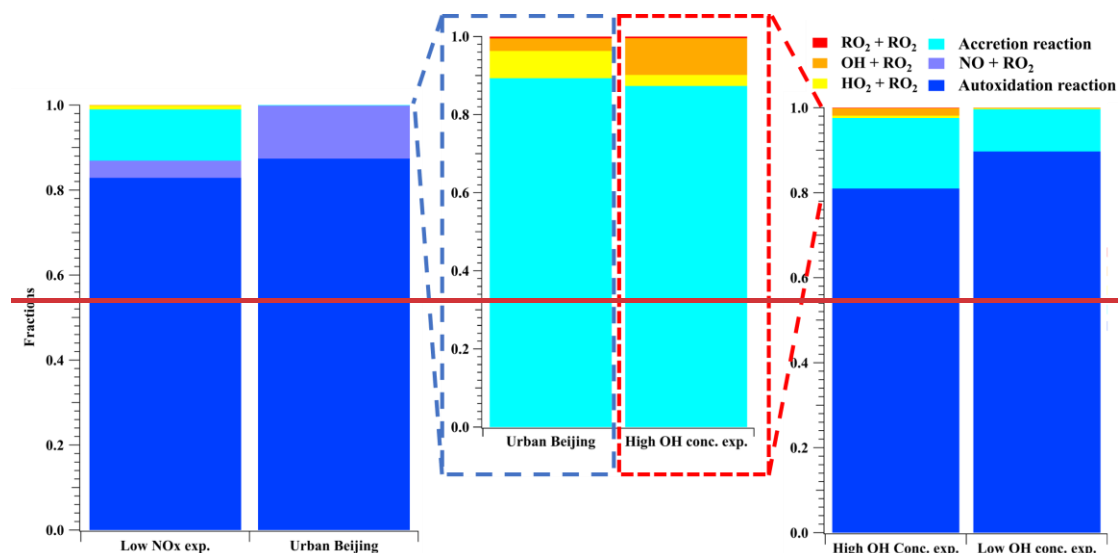
347

348 **Figure 1.** Fates of RO_2 generated in the low NO_x experiment (Exp. 44), urban Beijing (Slater

349 et al., 2020), low OH and zero NO_x experiment (Exp. 19), and high OH and zero NO_x

350 experiment (Exp. 12). Note that RO_2 fates of RO_2, OH, HO_2, and accretion channels are blown

351 up for a better comparison for urban Beijing and the high OH and zero NO_x experiment.

352 Reactions and kinetic rate coefficients used in the calculations are provided in Table S2.

353   Radical concentrations were also estimated by the PAM_chem_v8 model to illustrate the

354 chemical regimes in the 2nd-round experiments (Table S4). The average $[HO_2]$, $[OH]$, and $[RO_2]$

355 were 9.7×10^7, 1.64×10^7, and 1.69×10^9 molecule cm^{-3}, respectively, in Exp. 2-3, and were

356 6.7×10^7, 1.04×10^7, and 1.34×10^9 molecule cm^{-3}, respectively, in Exp. 2-4, both of which

357 generally differ by no more than a factor of 3 from the summer daytime ambient ones in polluted

358 atmosphere (Tan et al., 2017, 2018, 2019; Whalley et al., 2021; Lu et al., 2012). The average

359 $[HO_2]$, $[OH]$, and $[RO_2]$, as well as the NO and NO_2 concentrations in Exp. 2-7 are generally

360 very close to those in the same environment (Tan et al., 2019).

361 **(a)**
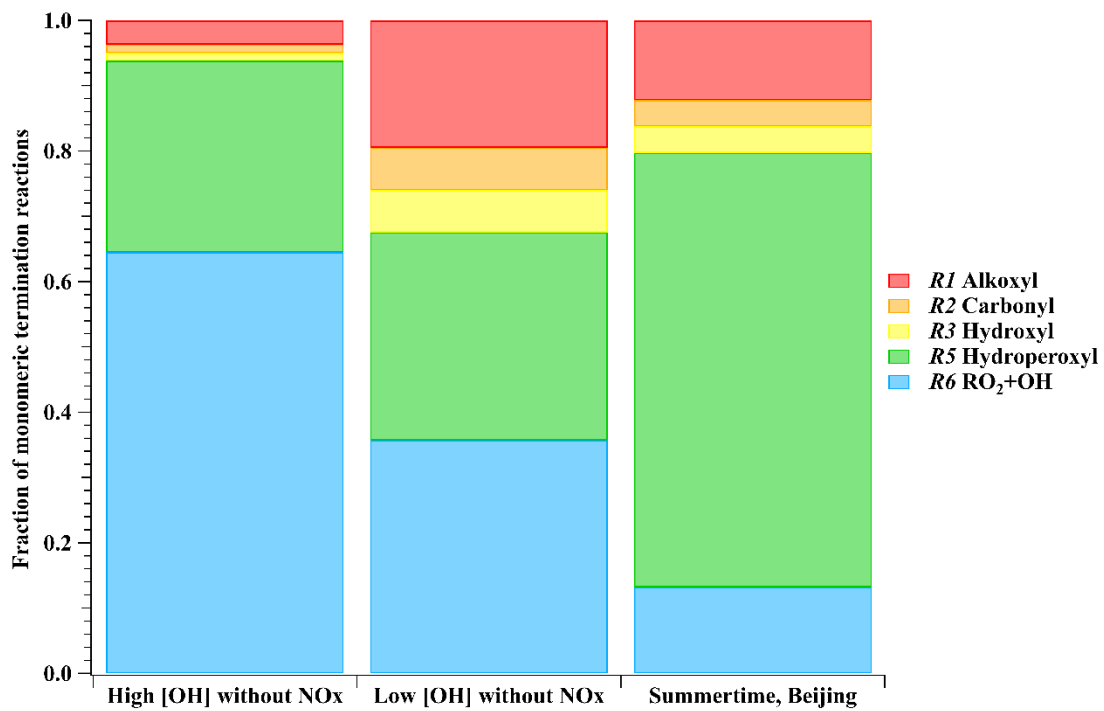
362

363 **(b)**
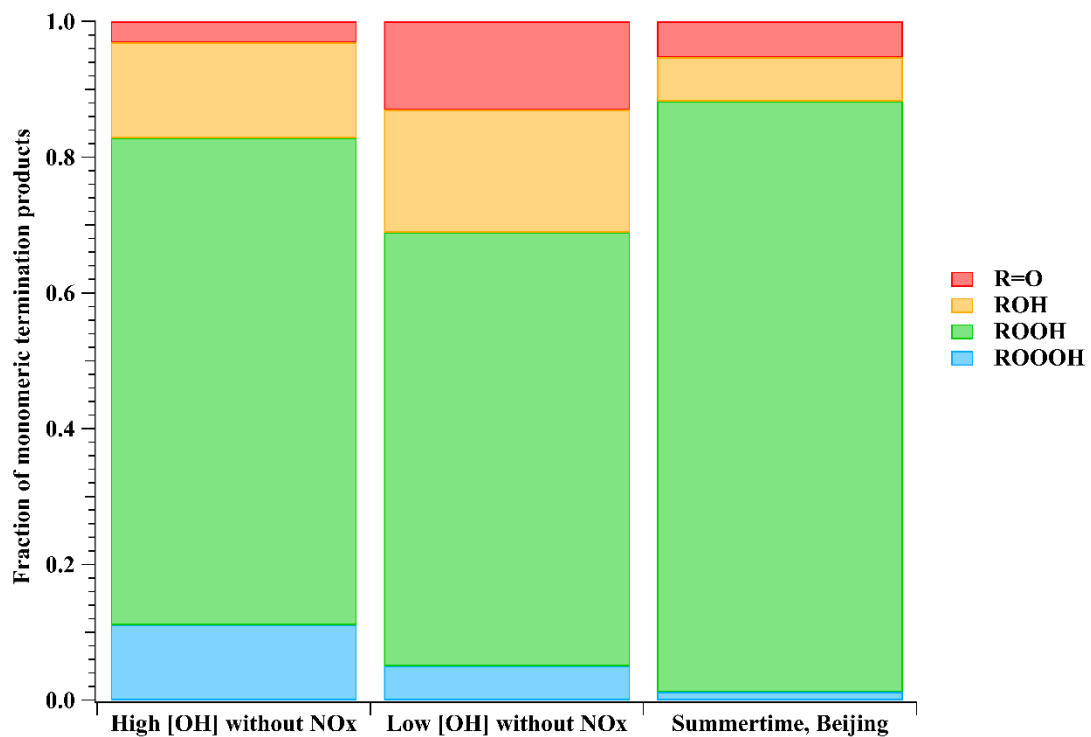
364

365 **(c)**

366

367 **(d)**

368
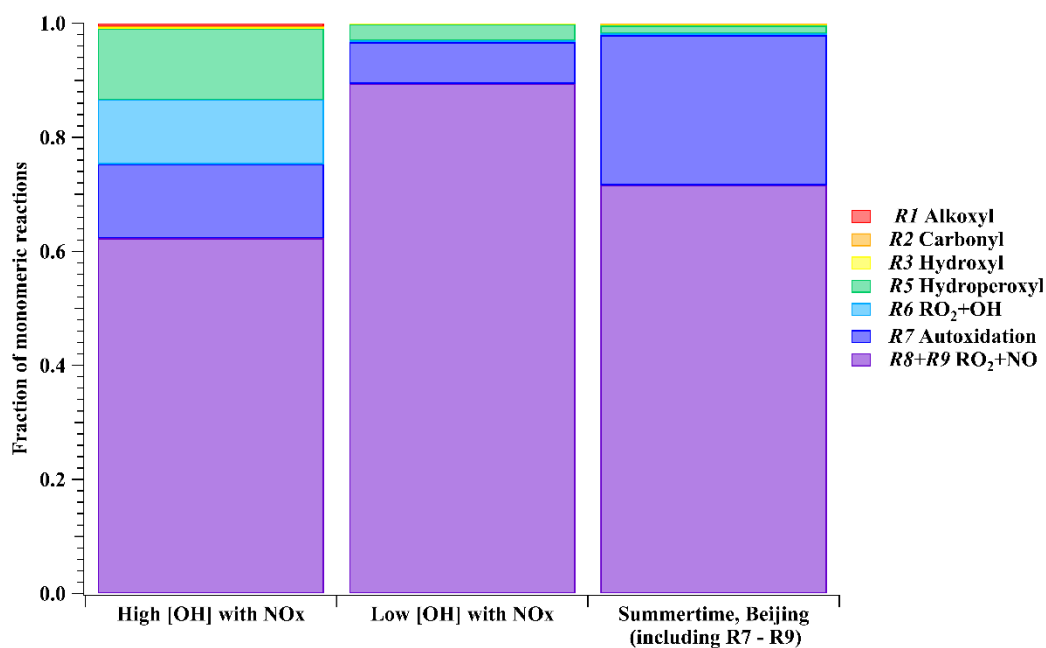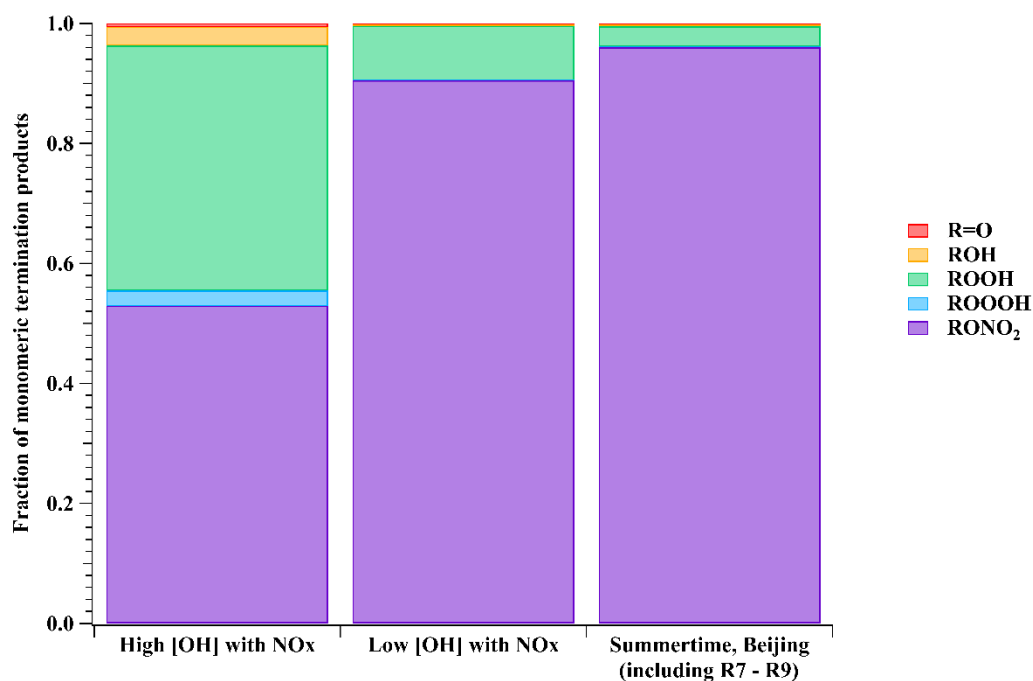
369 **Figure 1.** (a) The fraction of monomeric termination reactions and (b) monomeric termination

370 products of BPR in a representative high [OH] experiment without NO_x (Exp. 1-12), a

371 representative low [OH] experiment without NO_x (Exp. 2-3), and summertime, urban Beijing

372 (Whalley et al. 2021). NO_x related reactions and products for the Beijing study are not included

373 for a better comparison. (c) The fraction of monomeric reactions (R1 - R3 and R5 - R9) and (d)

374 monomeric termination products of BPR in a representative high [OH] experiment with NO_x

375 (Exp. 1-48), a representative low [OH] experiment with NO_x (Exp. 2-7), and summertime,

376 urban Beijing (Whalley et al. 2021). Reactions and kinetic rate coefficients used in the

377 calculations are provided in Table S2.

378 We take Exp. 1-12 ([OH] = ~8.47×10^8 molecule cm^{-3} and NO$_x$ = 0) and Exp. 2-3 ([OH] =

379 ~1.64×10^7 molecule cm^{-3} and NO$_x$ = 0) as representative examples and compare simulation

380 results with those from the ambient atmosphere, since NO$_x$ in the ambient is believed not to

381 impact relative ratios for $R1 - R3$, $R5$, and $R6$. In the ambient atmosphere, the average [HO$_2$],

382 [OH], and [RO$_2$] were 2.7×10^8, 8.0×10^6, and 1.4×10^9 molecule cm^{-3}, respectively, around

383 summertime noon in urban Beijing (Whalley et al. 2021), and (4 - 28)$\times10^8$, (0.8 - 2.4)$\times10^7$, and

384 1.2×10^9 molecule cm^{-3} (modeled) at a suburban site in Yangtze River Delta (Ma et al. 2022).

385 As shown in Figure 1a, for the most important RO$_2$, BPR, the fractions of monomeric

386 termination reactions of RO$_2$ + RO$_2$ ($R1 - R3$), RO$_2$ + HO$_2$ ($R5$), and RO$_2$ + OH ($R6$) were

387 6.2%, 29.3%, and 64.5%, respectively, in Exp.1-12. In contrast, the fractions were 32.5%,

388 31.8%, and 35.7%, respectively, in Exp. 2-3, whereas the values were 20.3%, 66.6%, and 13.2%,

389 respectively, for summertime, urban Beijing.

390 Our NO$_x$-free experiments are characterized with an inherent drawback that the proportion

391 of the HO$_2$ termination pathway ($R5$) is actually lower than that under ambient conditions,

392 which is similar to most other laboratory experiments (Bianchi et al., 2019). In our high [OH]

393 experiments without NO$_x$, the reaction rates of unimolecular reactions e.g., autoxidation

394 reaction ($R7$) and condensation ($R10$) did not change with [OH] that increased in our

395 experiments relative to that in the ambient. As a result, relative proportions of autoxidation and

396 condensation are lowered. On the other hand, 1,3,5-TMB-derived BPR was suggested to

397 undergo autoxidation ($R7$) at a reaction rate of 0.078 s^{-1} (Wang et al., 2017), which represents

398 36.8%, 94.4%, and 92.8% of the overall rates of $R1 - R3$ and $R5 - R7$ in Exp. 1-12, Exp. 2-3,

399 and summertime, urban Beijing, respectively. Because of its dominant proportion in Exp. 2-3

400 and the ambient, the autoxidation channel is not included for clarity in Figure 1a. Autoxidation

401 does possess a lower significance in our high [OH] experiments due to the other accelerated

402 bimolecular reactions. However, it would only influence the oxygen content of our products

403 but would not change the DBE. Both accretion reaction ($R4$) and condensation ($R10$) have been

404 taken into account in the model, but they would not influence the distributions of monomeric

405 stabilized products. We will specifically discuss these two pathways in the following sections

406 because of their complexity between the laboratory and ambient conditions.

407 RO$_2$ other than BPR and C$_9$H$_{13}$O$_7\cdot$ existed in the PAM OFR, which were not included in

408 the model simulation. Their reaction rates of the accretion reaction ($R4$) and the autoxidation

409 reaction ($R7$) should be different from BPR and C$_9$H$_{13}$O$_7\cdot$ due to the strong dependence of these

410 two reaction rates on the molecular structure. Rates for the other channels, on the other hand,

should be the same as those of BPR and $C_9H_{13}O_7\cdot$. Therefore, their fates in terms of the monomeric termination reactions ($R1$ - $R3$, $R5$ - $R6$, and $R8$ - $R9$) should be similar as BPR and $C_9H_{13}O_7\cdot$.

Calculated from yields of stabilized monomeric termination products of BPR, the fractions of monomeric termination reaction products in Exp. 1-12, Exp. 2-3, and summertime, urban Beijing (Whalley et al. 2021) are presented in Figure 1b, showing a lot of similarities between these conditions. The fractions of R=O, ROH, ROOH, and ROOOH in Exp. 1-12 were 3.1%, 14.1%, 71.7%, and 11.1%, respectively. These fractions were 13.0%, 18.1%, 63.9%, and 5.0%, respectively, in the Exp. 2-3, whereas the values were 5.3%, 6.5%, 87.0%, and 1.2%, respectively, in the summertime Beijing case. Among them, the majority of products are always ROOH and ROH, with ROOH being the most abundant. Therefore, the monomeric termination products of BPR in our experiments are atmospheric relevant. In addition, only the R=O product has a DBE higher than the reacted RO_2, but merely accounted for a limited proportion. All the other stabilized termination products have a DBE that is 1 lower than the precursor, and are the majority in both laboratory and ambient conditions. This indicates that the majority of the first-generation products typically have a DBE that is 1 lower than that of 1,3,5-TMB, whereas the majority of subsequent-generation products typically have a DBE that is 2 lower than that of 1,3,5-TMB. Once a monomeric compound with a DBE that is ≥2 lower than that of 1,3,5-TMB was observed, multi-generation OH reactions have happened in the system.

We take Exp. 12, 19 and 44 as representative examples and compare simulation results with those from the ambient environment (Slater et al., 2020). The RO_2 lifetime in urban Beijing (Slater et al., 2020), low NO_x experiment, low OH and zero NO_x experiment, and high OH and zero NO_x concentration experiment was 1.0, 0.7, 1.2, and 0.6 s, respectively. As shown in Figure 1, In the low NO_x experiment (Exp. 44), the fractions of RO_2 + RO_2 ($R1$ - $R3$), accretion reaction ($R4$), RO_2 + HO_2 ($R5$), RO_2 + OH ($R6$), autoxidation ($R7$), and RO_2 + NO ($R8$ - $R9$) were 0.06%, 12.1%, 0.9%, 0.07%, 82.9%, and 4.0%, respectively. Calculated based on the mean daytime peak concentrations of radicals in Beijing (Slater et al., 2020), the fractions of $R1$ - $R3$, $R4$, $R5$, $R6$, $R7$, and $R8$ - $R9$ were 0.0005%, 0.09%, 0.007%, 0.003%, 87.4%, and 12.5%, respectively. For the experiment with low OH and zero NO_x (Exp. 19), the fractions of $R1$ - $R3$, $R4$, $R5$, $R6$, and $R7$ were 0.05%, 10.0%, 0.15%, 0.14%, and 89.7%, respectively. For the one with high OH and zero NO_x (Exp. 12), the fractions of $R1$ - $R3$, $R4$, $R5$, $R6$, and $R7$ were 0.08%, 16.6%, 0.54%, 1.8%, and 81.0%, respectively. The overall lifetimes of RO_2 and the fractions of autoxidation together determine the significant and similar roles of autoxidation in both laboratory experiments and the ambient. Therefore, the autoxidation chain will run to a similar oxidation level between the laboratory and the ambient.

In experiments in absence of NO$_x$ (e.g., Exp.1-12), the proportions of $R8$ - $R9$, i.e., the NO channel in the urban atmosphere were attributed to termination reactions of $R1$ - $R6$, i.e., RO$_2$ + RO$_2$, accretion reaction, RO$_2$ + HO$_2$, and RO$_2$ + OH. By expanding proportions of these termination reactions, laboratory investigations on product distributions can be facilitated, as the detection of certain HOM products became more precise and the mass spectra became simplified.

In experiments with NO$_x$, the chemical fates of BPR in high [OH] experiments (Exp. 1-48 as an example, [OH] = ~6.77×10^8 molecule cm^{-3}, NO = ~1.93 ppb. NO$_2$ = ~68 ppb), low [OH] experiments (Exp. 2-7 as an example, [OH] = ~1.69×10^7 molecule cm^{-3}, NO = ~1.30 ppb. NO$_2$ = ~11 ppb), and the summertime, urban Beijing are compared. As shown in Figure 1c, in all three conditions, RO$_2$ reactions with NO were always the most significant pathway, with autoxidation being the second most significant.

Accounting for at least 52% of monomeric termination products under all conditions, organonitrates were always the most important termination products, as shown in Figure 1d. On the other hand, based on the formulae of organonitrates, the detailed formulae for monomer RO$_2$ could be probed, which can help us better understand the chemical reactions inside the system. In experiments with NO$_x$ (e.g., Exp. 44), though the yields of organonitrates were lower in the laboratory experiments, the formation pathways of these compounds were the same as those in the ambient. Based on the formulae of organonitrates, the detailed formulae for monomer RO$_2$ could be probed, which helps to investigate the existence of multi-generation OH oxidation. Alkoxy radicals generated in the NO termination channel will unlikely influence the distributions of C9 stabilized products since they tend to get decomposed in the subsequent reactions, as discussed in the Supplementary Text S1.

In experiments in absence of NO$_x$ (e.g., Exp. 12 and 19), the proportions of $R8$ - $R9$, i.e., the NO channel in urban environment were reassigned to termination reactions of $R1$ - $R6$, i.e., RO$_2$ + RO$_2$, accretion reaction, RO$_2$ + HO$_2$, and RO$_2$ + OH. Comparison of relative fractions of RO$_2$ fates of RO$_2$, OH, HO$_2$, and accretion channels (Figure 1) shows similarities between laboratory and ambient results. By expanding proportions of these termination reactions, laboratory investigations on distributions of products can be facilitated, as the detection of certain HOM products became more precise and the mass spectra became simplified. As discussed in the "results" session, products of $R2$, $R3$, and $R5$ channels of the main BPR were not detected in our experiments due to their low oxygen contents, while secondary products between products of $R2$, $R3$, and $R5$ channels of the main BPR and OH were observed. Together with stabilized products and secondary products from C$_9$H$_{13}$O$_7$· (the peroxy radical formed from autoxidation of BPR), secondary products between products of $R2$, $R3$, and $R5$

481 ~~channels of the main BPR and OH help to elucidate the first- and multi-generation reaction~~

482 ~~pathways in the 1,3,5-TMB+OH system, according to their molecular formular.~~

483 ~~On the other hand, t~~ Due to the complexity of ambient RO_2 pool, it is difficult to estimate

484 the detailed fraction of accretion reactions $R4$. In the laboratory experiments, RO_2 pool mainly

485 consists of BPR and its autoxidation reaction product $C_9H_{13}O_7\cdot$, which both can undergo

486 accretion reaction rapidly (Berndt et al., 2018b). The concentrations of these two radicals were

487 estimated by PAM_chem_v8 according to the kinetics discussed in Supplementary Text S1. The

488 reaction rate of accretion ($R4$) for BPR was around 1.61 s^{-1} in Exp.1-12, being 61.8% of $R1 -$

489 $R7$, and was 0.29 s^{-1} in Exp.2-3, equivalent to 21.1% of $R1 - R7$. Certain uncertainties exist

490 in the estimation of the proportions of accretion reactions, as the PAM_chem_v8 model only

491 includes the first-generation reactions of precursors, whereas the subsequential fragmentation

492 and re-initiation of stabilized products can generate a series of new RO_2 that will influence the

493 proportions of accretion reactions. We are only certain that the significance of accretion

494 reactions in both Exp. 1-12 and Exp. 2-3 is larger than the ambient. The much-expanded

495 proportion of HOM dimers through accretion reactions makes it inadequate to compare yields

496 of HOM dimers and HOM monomers. However, this deviation will not influence our

497 conclusion on multi-generation OH oxidation and identification of HOM dimers can help us

498 identify the exact RO_2 in the OFR and confirm the conditions of secondary OH oxidation

499 according to the number of hydrogen atoms in the molecules.

500 In addition, certain compounds might have condensed onto pre-existing particles in the

501 real atmosphere before an appreciable fraction of such compounds undergoes the re-initiated

502 OH oxidation. Therefore, even the same product can be generated both in the laboratory

503 experiments and the ambient atmosphere, the relative significance of this product is not

504 completely identical. Though OOMs might have the potential to undergo multi-generation OH

505 oxidation, the exact proportion of this reaction in the ambient strongly depends on their

506 volatility, in other words, condensation sink of these OOMs. The typical monomeric

507 termination products of 1,3,5-TMB-derived BPR, $C_9H_{12}O_4$, $C_9H_{14}O_4$, $C_9H_{14}O_5$, and $C_9H_{13}NO_6$,

508 are estimated to have saturation vapor concentrations (C*) of 30.20, 30.20, 0.85, and 3.39 μg/m^3

509 at 300 K with the volatility parameterization developed in the CLOUD chamber oxidation

510 experiments of aromatics, respectively (Wang et al., 2020a). From the perspective of volatility,

511 they all belong to semi-volatile organic compounds (SVOC, 0.3 < C* < 300 μg/m^3) and are

512 expected to exist in both the condensed and the gas phases at equilibrium in the atmosphere

513 (Bianchi et al., 2019). Compared to ambient conditions, their condensation rates in the

514 laboratory were biased to be lower due to the accelerated bimolecular reactions. However, this

515 will not prevent the high [OH] experiments from showing the potential and ability of these

516 compounds to go through re-initiated OH oxidation, as these compounds would exist in
517 significant fractions in the gas phase in the real atmosphere.
518   However, the conditions are completely distinct for other HOM monomer products and
519 HOM dimer products with much lower volatility. It is difficult for a HOM dimer, e.g., $C_{18}H_{26}O_{10}$
520 estimated with a C^* of 7.24×10^{-13} μg/m^3 at 300 K, to survive long enough to experience an
521 appreciable re-initiated photochemical ageing. The lifetime of HOMs that can be classified as
522 LVOCs ($3 \times 10^{-5} < C^* < 0.3$ μg/m^3) and ELVOCs ($C^* < 3 \times 10^{-5}$ μg/m^3) can be estimated
523 according to the condensation sink (CS) in the atmosphere, as they are lost irreversibly onto
524 surfaces. The median value of CS in urban Beijing was reported to be around 0.019 s^{-1} and
525 0.057 s^{-1} during NPF days and non-NPF days, respectively, whereas the values in Shanghai
526 were reported to be around 0.013 s^{-1} and 0.017 s^{-1}. respectively (Deng et al., 2020; Yao et al.,
527 2018), which are all much higher than the physical loss in our PAM OFR, i.e., 0.0023 s^{-1}, as
528 stated in the Supplementary Text S1. LVOCs and ELVOCs are believed to be lost irreversibly
529 to the surface in both the laboratory and ambient because of their low volatility. However, by
530 assuming a similar diffusion coefficient of LVOCs and ELVOCs to that of sulfuric acid, the
531 lifetimes of LVOCs and ELVOCs in the ambient still can be as high as 77 s for the condensation
532 loss, which is close to the residence time of our PAM OFR. Therefore, LVOCs and ELVOCs
533 should at least have the potential to experience the same OH exposures in the ambient as those
534 in our low [OH] experiments, i.e., at least 5.86×10^8 molecule cm^{-3} s, if they were generated. On
535 the other hand, the detailed proportions of LVOCs and ELVOCs after a large OH exposure
536 should be lower than those in the lab due to their magnified physical loss in the ambient. This
537 means that if the multi-generation products of those compounds were observed in the ambient
538 air, they should have been generated via a reaction that happened very recently.

3.2 Oxidation products in high [OH] experiments

540   A total of 33 HOM monomers with formulae of $C_{7-9}H_{8-16}O_{6-11}$ and 22 HOM dimers with
541 formulae of $C_{17-18}H_{24-30}O_{8-14}$ were observed in the 1st-round experiments of gas phase OH-
542 initiated oxidation of 1,3,5-TMB in the OFR, i.e., high [OH] experiments, as listed in Table
543 S4S5. The relative signal contributions of HOMs to the total signals of all HOMs at an OH
544 exposure of 2.38×10^{10} molecules cm^{-3} s are listed as an example in Table S4S5. The most
545 abundant HOM products were also shown in stack in Figure 2, whose relationships with OH
546 exposures are superimposed by a gamma function ($f(x) = ax^m e^{-x}$) simulation line to guide
547 the eyes. The sum of normalized HOM monomers' abundance increased monotonically up to
548 the highest OH exposure of 5×10^{10} molecule cm^{-3} s, whereas those of HOM dimers showed a
549 non-monotonic dependence on OH exposure. The observed faster increase of accretion
550 products than that of HOM monomers can be explained jointly by the fast second-order kinetics

551 for accretion reactions of RO$_2$ (Berndt et al., 2018b) and the high concentrations of relevant

552 radicals in this work. On the other hand, most of the first-generation HOM dimers formed from

553 accretion reactions contain at least one C=C bond and have more functionalities than HOM

554 monomers, and thus should be more reactive to OH radicals, which, together with a faster

555 deposition loss of dimers, results in a faster consumption of HOM dimers than monomers in

556 the OFR. The faster production and consumption of HOM dimers allowed their concentrations

557 to summit at middle levels of OH exposures. As stated in Section 3.1, Bbecause of the inherent

558 disadvantage of laboratory experiments, [RO$_2$] concentrations are is always too high in the OFR,

559 which has been pointed out in a previous study (Bianchi et al., 2019). The accretion reactions

560 in the OFR are relatively more significant than it should be in the ambient atmosphere. We do

561 not mean to compare HOM monomer and HOM dimer signals crossly here, but to pay attention

562 to their formulae.

563 (a)

564
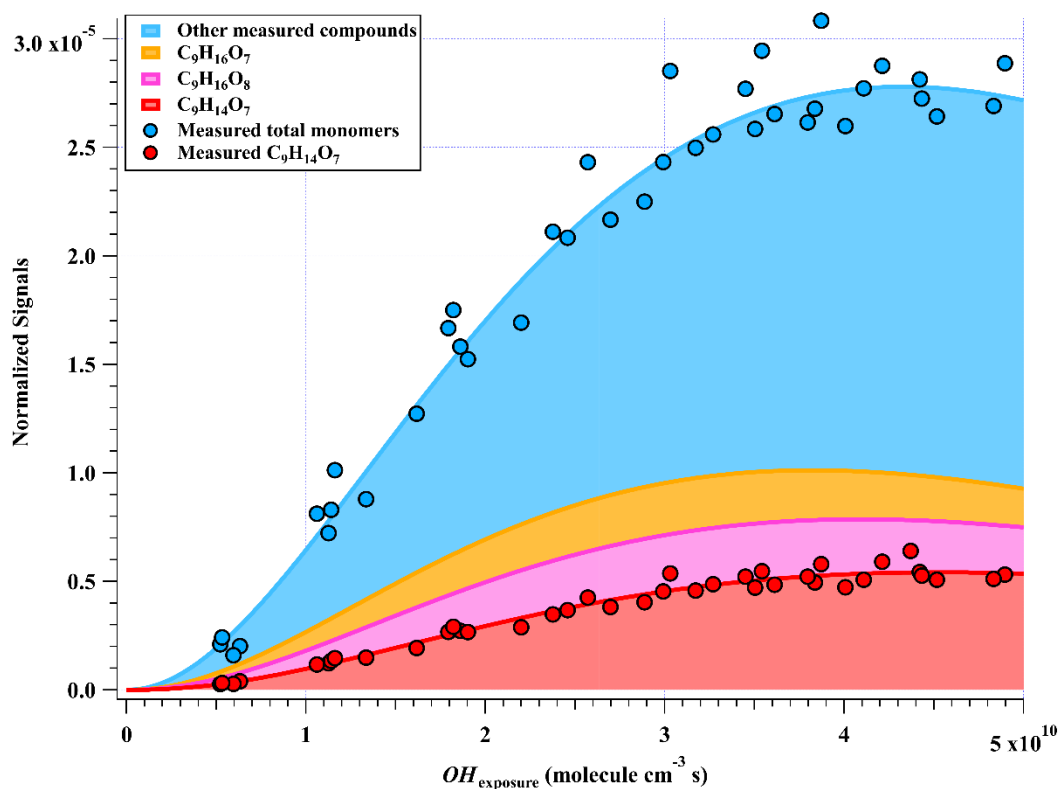
565 (b)
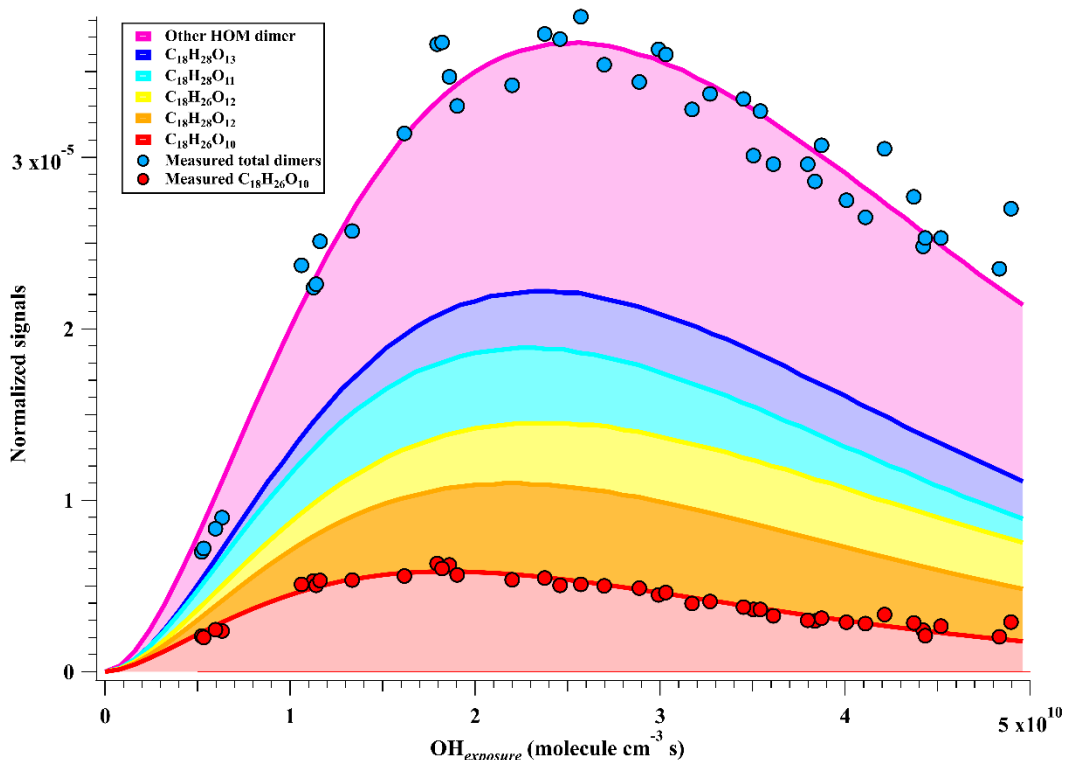
Figure 2. Normalized signals of (a) HOM monomers and (b) HOM dimers versus OH exposure in the high [OH] experiments, whichthat are fitted via a gamma function and shown in stacked.

Theoretically, at a given RH and UV (i.e., a given [OH]), an increase in the initial TMB would lead to formation of more RO_2, which corresponds to a larger RO_2/OH. However, under our high [OH] experimental conditions, the RO_2/OH/HO_2 channels of RO_2 radicals are always minor, and thus an increase in RO_2/OH would not have a significant impact on the relative distribution of products formed from these channels. We compared product MS for experiments with a similar OH exposure but different initial concentrations of TMB (e.g., Exp. 1-3 v.s. Exp. 1-19, and Exp. 1-12 v.s. Exp. 1-22). The OH exposures of Exp. 1-3 and Exp. 1-19 were estimated by the modified PAM_chem_v8 modelconsumption of precursors to be 5.2×10^9 and 5.3×10^9 molecule cm^{-3} s, respectively, but the initial concentration of TMB of Exp. 1-3 was 25% more than that in Exp. 1-19. Meanwhile, the OH exposures of Exp. 1-12 and Exp. 1-22 were 4.5×10^{10} and 4.4×10^{10} molecule cm^{-3} s, respectively, but the initial concentration of TMB of Exp. 1-12 was 48% more than that in Exp. 1-22. Comparisons between the product MS of Exp. 1-3 and Exp. 1-19 (Figure S2), as well as of Exp. 1-12 and Exp. 1-22, show that increase in the initial concentration of precursors generally resulted in a minor increment in the absolute signals of HOMs. Clearly, the relative distributions of products in these experiments are quite similar, indicating a minor difference in the relative distributions of products caused by fluctuations of initial concentrations of TMB.

587   3.2.1 HOM monomers

588   Previous studies indicate that oxidation products derived from the peroxide-bicyclic

589 pathway represent a main fraction of HOMs (Wang et al., 2017; Zaytsev et al., 2019). For 1,3,5-

590 TMB, this pathway, as recommended by Master Chemical Mechanism (MCM), starts from a

591 BPR, $C_9H_{13}O_5\cdot$ (MCM name: TM135BPRO2) (Molteni et al., 2018). According to MCM and

592 Molteni et al. (2018), Scheme 1 has been proposed to provide a good understanding of this

593 reaction system and the structures of oxidation products. Molteni et al. (2018) suggested that

594 $C_9H_{13}O_7\cdot$, i.e., peroxy radical formed from autooxidation of $C_9H_{13}O_5\cdot$ has two isomers. A

595 second-step of endo-cyclization is required in the formation of one of the isomer, which is

596 extremely slow and not competitive as shown in several previous studies using both

597 experimental and theoretical approaches (Wang et al., 2017; Xu et al., 2020). Even if such a

598 second O_2 bridging to a double bond is assumed to be possible, the abundance of this isomer

599 should be significantly smaller than the other one, because of the much faster reaction rate of

600 H-shift reaction. Therefore, we do not take the $C_9H_{13}O_7\cdot$ isomer containing a double endo-

601 cyclization into consideration in this work. The majority of HOM monomers is generated from

602 subsequent reactions of $C_9H_{13}O_5\cdot$ and newly formed $C_9H_{13}O_7\cdot$, both of which contain one C=C

603 bond in the carbon backbone and thus have a feasible site for OH addition. Meanwhile, the

604 autoxidation reaction rate for newly formed $C_9H_{13}O_7\cdot$ should be significantly smaller than

605 $C_9H_{13}O_5\cdot$, as there is no hydrogen atom in $C_9H_{13}O_7\cdot$ that is able to undergo a hydrogen atom

606 shift at an appreciable rate based on our current understanding. Therefore, the subsequent

607 autoxidation reaction should not be able to generate large amounts of more oxidized RO_2.
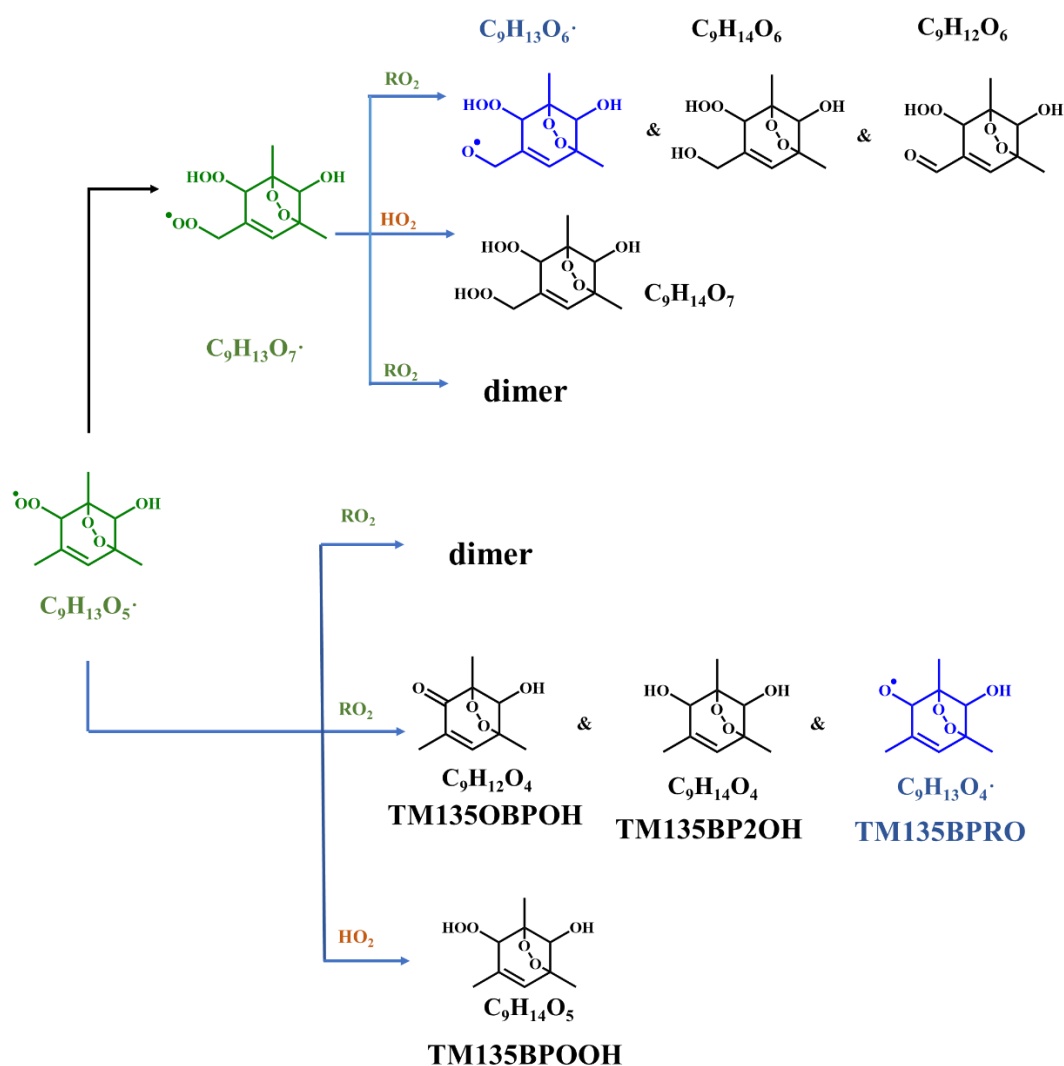
Scheme 1. Oxidation pathways of the bicyclic peroxy radical $C_9H_{13}O_5\cdot$ (MCM name: TM135BPRO2) in the OH-initiated oxidation of 1,3,5-TMB. Green, blue, and black formulae denote alkyl peroxy radicals, alkoxy radicals and stabilized products, respectively. Black arrows denote the autoxidation pathway. MCM names for HO_2- and RO_2-termination products of TM135BPRO2 are present.

Monomeric termination products of BPR, as shown in Scheme 1, were not detected by nitrate CIMS in this round of experiments, which might be due to the fast sub-sequential OH oxidation of these products under high [OH] environment~~due to their own low oxygen content and thus relative low detection efficiency in nitrate CIMS, which has been investigated in a previous study (Riva et al., 2019)~~ since they were observed under low [OH] environments as shown in Section 3.3. Monomeric termination products~~Those~~ of $C_9H_{13}O_7\cdot$ were all observed clearly, including $C_9H_{12}O_6$, $C_9H_{14}O_6$, and $C_9H_{14}O_7$. Especially, $C_9H_{14}O_7$ was the most abundant one among all of the HOM monomer products (Figure 2a). As proved by a previous study, these

622   three species should be typical first-generation stabilized products derived from autoxidation

623   (Wang et al., 2020b). These HOM monomers should consist of several isomers bearing the

624   same formula, because products from the secondary reactions cannot share the same structure

625   as that of the one from the first-generation reaction. However, limited by the inherent

626   disadvantages of mass spectrometers, we could not distinguish isomers here and further

627   illustrate their different chemical behaviors.

628   In addition to these three ones, the next most prominent products to $C_9H_{14}O_7$ were $C_9H_{16}O_7$

629   and $C_9H_{16}O_8$ (Figure 3a), which are produced from multi-generation oxidation according to

630   their ~~hydrogen content~~DBE ~~(Molteni et al., 2018; Cheng et al., 2021)~~. Based on the formulae

631   of these three HOM monomers, they ($C_9H_{14}O_7$, $C_9H_{16}O_7$, and $C_9H_{16}O_8$) could be formed from

632   the bimolecular termination reactions of $C_9H_{15}O_8{}^\bullet$, which can be generated by an OH attack to

633   $C_9H_{14}O_5$ (Scheme 2), the hydroperoxyl termination product of the BPR, $C_9H_{13}O_5{}^\bullet$. The other

634   HOM monomers characterized with high signals were $C_9H_{14}O_8$ and $C_9H_{16}O_9$ (Figure 3b). These

635   two HOM monomers ($C_9H_{14}O_8$ and $C_9H_{16}O_9$), together with $C_9H_{16}O_8$, correspond to the

636   monomeric termination products of $C_9H_{15}O_9{}^\bullet$, which is highly likely the peroxy radical

637   generated by an OH attack to $C_9H_{14}O_6$ (Scheme 3), i.e., the hydroxyl termination product of

638   $C_9H_{13}O_7{}^\bullet$. As discussed earlier, $C_9H_{13}O_7{}^\bullet$ is a typical autoxidation reaction product of the BPR

639   of $C_9H_{13}O_5{}^\bullet$. Therefore, detected signals of $C_9H_{16}O_8$ should be the sum of two isomers' signals

640   at least. Other HOM monomers were generally observed at much lower signals and thus were

641   not plotted individually.

642   (a)
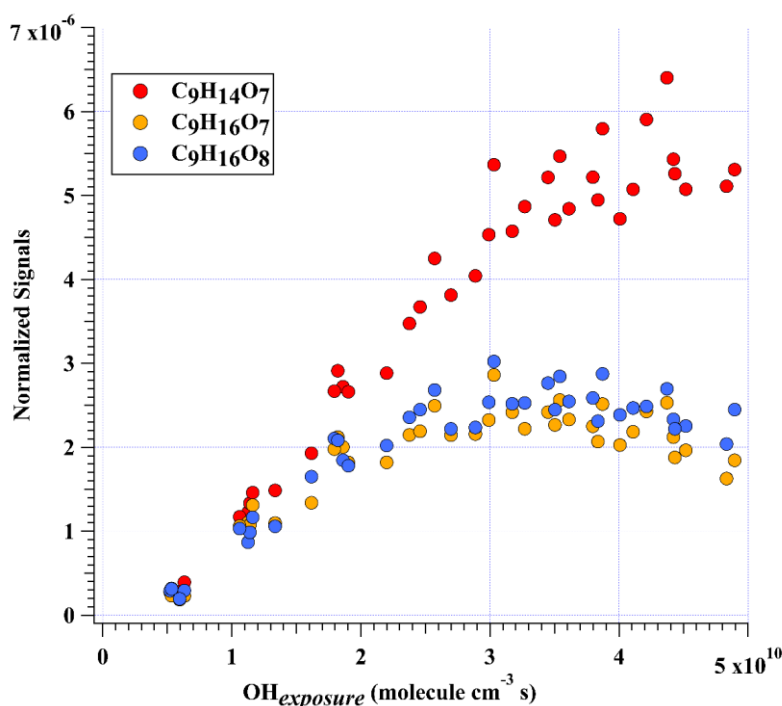
643

644   (b)
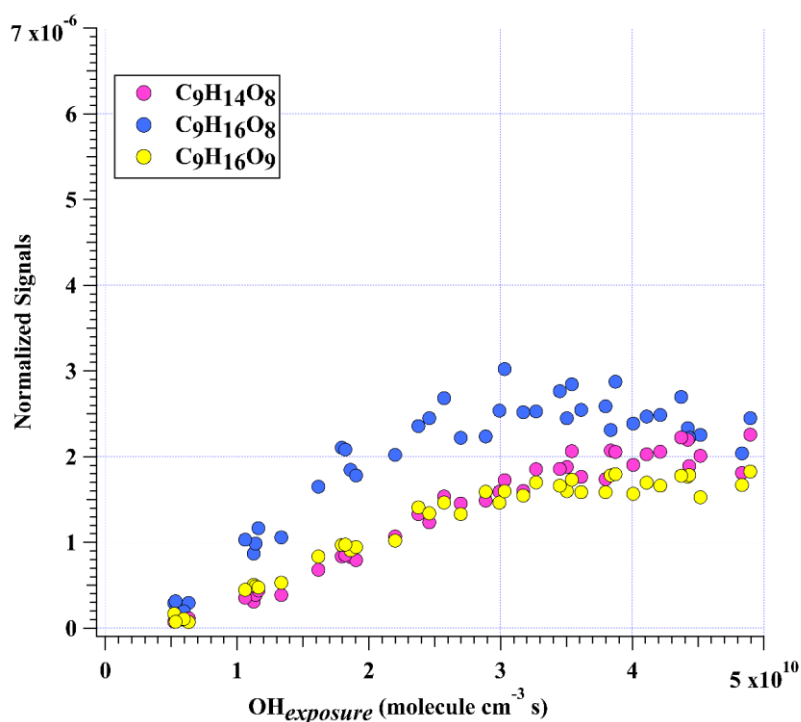
645

646   **Figure 3.** Normalized signals of (a) $C_9H_{14}O_7$, $C_9H_{16}O_7$, and $C_9H_{16}O_8$ and (b) $C_9H_{14}O_8$, $C_9H_{16}O_8$,

647   and $C_9H_{16}O_9$ measured at the exit of OFR in our high [OH] experiments without NO_x as a

648   function of OH exposure. $C_9H_{16}O_8$ are shown in both plots to better illustrate the chemical

649   profiles of different compound groups.
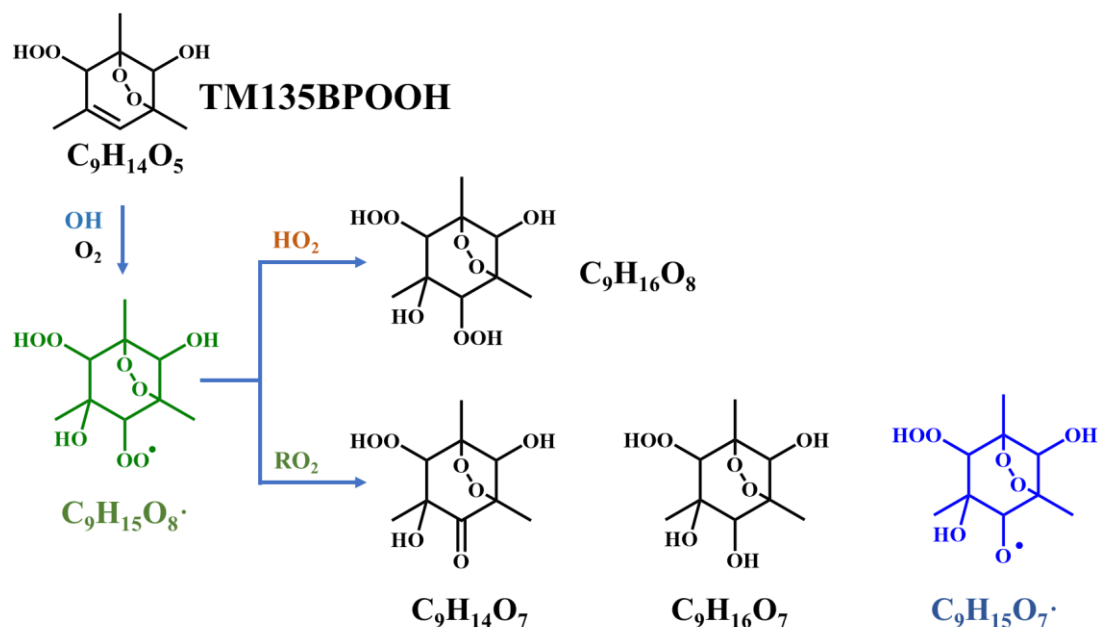
650

651   **Scheme 2.** Proposed formation pathways of $C_9H_{14}O_7$, $C_9H_{16}O_7$, and $C_9H_{16}O_8$ via the secondary

652   OH oxidation of TM135BPOOH.

653
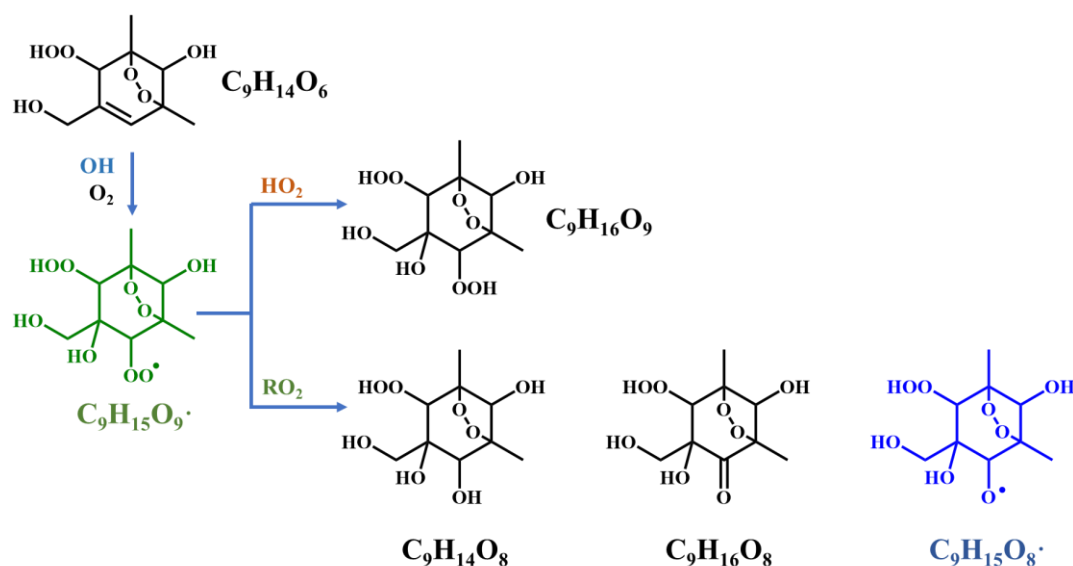
Scheme 3. Proposed formation pathways of $C_9H_{14}O_8$, $C_9H_{16}O_8$, and $C_9H_{16}O_9$ via the secondary OH oxidation of TM135BPOOH.

It is worth noting that HOM monomers with 18 hydrogen atoms, i.e., a DBE of 1, were never observed in our experiments, including a potential stabilized hydroperoxyl products formed from $C_9H_{17}O_m\cdot$. This is expected, since $C_9H_{17}O_m\cdot$ should be in really low concentrations, if ever existed. As indicated by its hydrogen number, a $C_9H_{17}O_m\cdot$ was formed by at least two OH additions to the C=C bond of a $C_9H_{13}O_m\cdot$, but the main BPR, $C_9H_{13}O_5\cdot$, and its autoxidation product ($C_9H_{13}O_7\cdot$), are characterized with one C=C bond on the ring, which makes this formation pathway impossible. Other ring-breakage pathways should not contribute to the formation of this radical ($C_9H_{17}O_m\cdot$) because of their low branching ratio as determined by recent studies (Zaytsev et al., 2019; Xu et al., 2020).

Proposed according to MCM and Molteni et al. (2018), ~~Scheme~~ scheme 4 shows the NO termination pathways of the main BPR $C_9H_{13}O_5\cdot$ and its autoxidation product, $C_9H_{13}O_7\cdot$. After introducing N_2O into PAM OFR, quantities of organonitrates were generated, including both C9 and C18 organonitrates. The averaged mass spectrometry of nitrate CIMS in the 1.8 ppb NO experiment and 4.8 ppb NO experiment is shown in Figure S3. Organonitrates were formed via the NO + RO_2 reaction, called as NO termination reactions. The distribution of oxidation products under these two NO settings were similar.
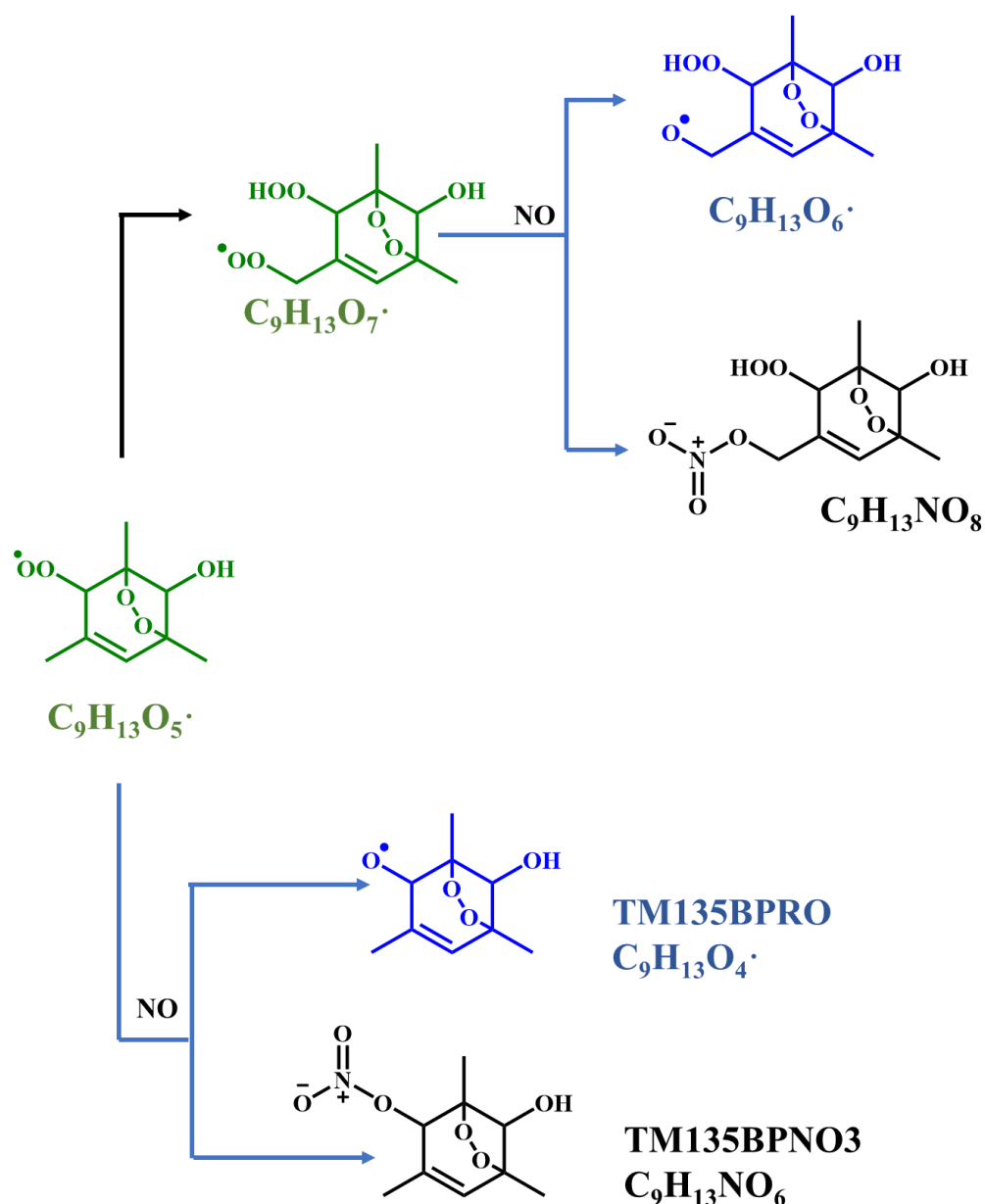
Scheme 4. NO termination reactions of the bicyclic peroxy radical $C_9H_{13}O_5\cdot$ (MCM name: TM135BPRO2) and its autoxidation reaction products. Green, blue, and black formulae denote alkyl peroxy radicals, alkoxy radicals and stabilized products, respectively. Black arrows denote the autoxidation pathway. MCM names of NO-termination products of TM135BPRO2 are present.

As discussed above, most of the first-generation HOMs should contain a C=C bond in the carbon backbone. The ubiquitous existence of organonitrates that contain two nitrogen atoms exactly confirms the extensive secondary OH oxidation in the systems, because the NO termination reaction of RO_2 is the only pathway that can generate organonitrates in our experiments and this pathway can only introduce one nitrogen atom at a time, as indicated in Scheme 4. RO_2 can react with NO_2 to form peroxynitrates (ROONO$_2$) but these species are

684 thermally unstable except at very low temperatures or when the RO_2 is an acylperoxy radical
685 (Orlando and Tyndall, 2012), neither of which were not met in our experiments. The
686 concentrations of NO_3 were estimated to be lower than 1 pptv by our modified PAM_chem_v8
687 because of the existence of decent concentrations of NO, which would consume NO_3 at a rapid
688 reaction rate, i.e., 2.7×10^{-11} molecule^{-1} cm^3 s^{-1} (IUPAC dataset , https://iupac-aeris.ipsl.fr, last
689 access: 26 October 2023). Therefore, NO_2 and NO_3 were not likely to react with RO_2 to form
690 large amounts of organonitrates in our experiments. Taking the most abundant organonitrate,
691 $C_9H_{14}N_2O_{10}$, as an example, it was exactly the NO termination product of $C_9H_{14}NO_9\cdot$, which
692 was generated from an OH attack and a subsequent O_2 addition to $C_9H_{13}NO_6$, the NO
693 termination product of $C_9H_{13}O_5\cdot$. For other organonitrates, $C_9H_{13}NO_8$, the second most
694 abundant organonitrate, could be either a NO termination product of $C_9H_{13}O_7\cdot$ or, together with
695 other most abundant organonitrates, $C_9H_{15}NO_7$ and $C_9H_{15}NO_8$, classical termination products
696 of $C_9H_{14}NO_9\cdot$. $C_9H_{14}N_2O_{10}$, $C_9H_{15}NO_7$, and $C_9H_{15}NO_8$ all have a DBE of 2 lower than the
697 precursor and thus are the typical multi-generation OH oxidation products.

698   The NO:RO_2 ratio in the PAM OFR in this series of experiments is lower than typical
699 values in the ambient atmosphere, which is due to the existence of O_3 that was utilized to
700 generate O(^{1}D) in the OFR and its rapid reaction rate with NO. However, due to rapid reaction
701 rate constants between NO and RO_2, i.e., around 8.5×10^{-12} molecule^{-1} cm^3 s^{-1}, the reaction rate
702 for the NO termination channel of RO_2 was as fast as around $0.3 – 1.0$ s^{-1}. Large amounts of
703 organonitrates would still be formed, as discussed in Section 3.1. Our conclusion is also valid
704 because of detection of compounds with multiple nitrogen atoms.

705   3.2.2 HOM dimers

706   Accretion reaction $RO_2 + RO'_2 \rightarrow ROOR' + O_2$ is a source of gas-phase dimer
707 compounds from highly oxidized, functional RO_2 radicals (Ehn et al., 2014; Berndt et al., 2018b;
708 Zhao et al., 2018; Berndt et al., 2018a). $C_{18}H_{26}O_8$ and $C_{18}H_{26}O_{10}$ are two typical accretion
709 reaction products in the 1,3,5-TMB + OH system, whose formation pathways have been
710 elucidated (Berndt et al., 2018b). $C_{18}H_{26}O_8$ can only be formed via the accretion reaction of two
711 $C_9H_{13}O_5\cdot$. $C_9H_{13}O_3\cdot$ is not likely to react with $C_9H_{13}O_7\cdot$ to form large amounts of $C_{18}H_{26}O_8$.
712 $C_9H_{13}O_3\cdot$ can only be formed after addition of a hydroxyl radical to the aromatic ring of 1,3,5-
713 TMB and a subsequent O_2 addition to the newly formed hydroxyl-substituted cyclohexadienyl
714 radical (Vereecken, 2019). However, the lifetime of this radical is extremely short, as $C_9H_{13}O_3\cdot$
715 will undertake a ring-closure reaction and get attached by a O_2 very rapidly, forming BPR,
716 $C_9H_{13}O_5\cdot$. Its short lifetime and low concentration, as indicated by Berndt et al. (2018), lead to
717 its insignificant role in the accretion reactions. In contrast, $C_{18}H_{26}O_{10}$ can be formed either by
718 the accretion reaction between $C_9H_{13}O_5\cdot$ and $C_9H_{13}O_7\cdot$ or via a second OH attack to $C_{18}H_{26}O_8$.

719 These two HOM dimers are so far the only ones that are confirmed to be formed via the

720 accretion reactions (Berndt et al., 2018b; Bianchi et al., 2019). ~~There are currently no evidences~~

721 ~~supporting that $C_9H_{15}O_m\cdot$ radicals can participate in the formation of HOM dimers with 28~~

722 ~~hydrogens. Therefore, it hints that one could attribute the formation of $C_{18}H_{28}O_m$ to multi-~~

723 ~~generation OH oxidation of $C_{18}H_{26}O_m$.~~

724 $C_{18}H_{26}O_{10}$ was characterized with the highest dimer signals for experiments with OH

725 exposures under 3.5×10^{10} molecule cm^{-3} s. Nevertheless, $C_{18}H_{26}O_{10}$, together with $C_{18}H_{28}O_{12}$,

726 $C_{18}H_{26}O_{12}$, $C_{18}H_{28}O_{11}$, $C_{18}H_{28}O_{13}$, and $C_{18}H_{28}O_{10}$ contributed more than 50% of total HOM

727 dimer signals at any OH exposure levels (Figure 2b). These six most abundant HOM dimers

728 correspond exactly to the hydroperoxyl, hydroxyl, and carbonyl termination products of

729 $C_{18}H_{27}O_{11}\cdot$ and $C_{18}H_{27}O_{13}\cdot$, respectively. These two RO$_2$ ($C_{18}H_{27}O_{11}\cdot$ and $C_{18}H_{27}O_{13}\cdot$), on the

730 other hand, could be generated by OH attacks to $C_{18}H_{26}O_8$ and $C_{18}H_{26}O_{10}$, respectively, which

731 strongly suggests the significant role of secondary OH chemistry in the formation of HOMs in

732 our experiments. In addition, $C_{18}H_{28}O_x$ can also be formed through accretion of a $C_9H_{13}O_m\cdot$

733 radical and a $C_9H_{15}O_m\cdot$ radical, as suggested by previous studies (Molteni et al., 2018;

734 Tsiligiannis et al., 2019). However, since a $C_9H_{15}O_m\cdot$ radical, as suggested by its hydrogen atom

735 number, can only be formed via an OH addition to the stabilized $C_9H_{14}O_m$ products through

736 multi-generation OH reactions, our conclusion that $C_{18}H_{28}O_x$ are multi-generation OH

737 oxidation products still holds. Figure 4 shows the normalized signals of these abundant HOM

738 dimers at different OH exposures.

739 (a)
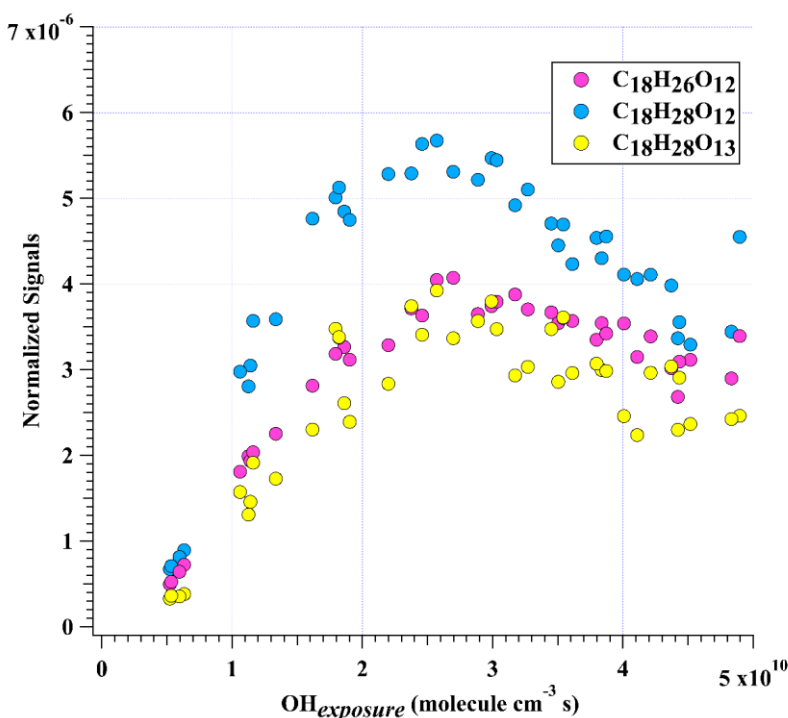
740

741   (b)
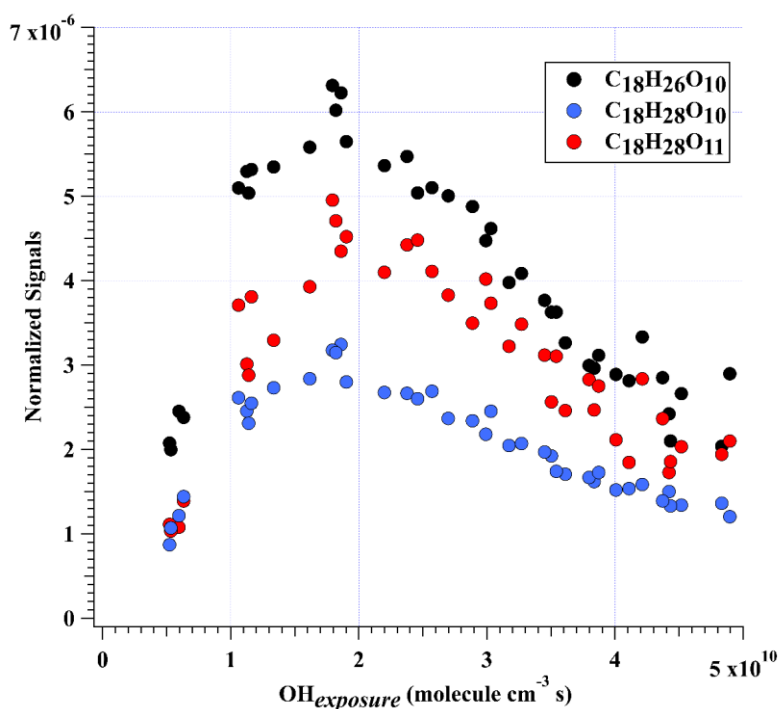
742

743   **Figure 4.** Normalized signals of (a) $C_{18}H_{26}O_{12}$, $C_{18}H_{28}O_{12}$, and $C_{18}H_{28}O_{13}$, and (b) $C_{18}H_{26}O_{10}$,
744    $C_{18}H_{28}O_{10}$, and $C_{18}H_{28}O_{11}$ measured at the exit of OFR in our high [OH] experiments without
745   NO_x as a function of OH exposure.

746   This decrease of dimer at relatively high OH exposures are likely due to the accelerated
747   accretion reactions in the OFR, resulted by the high RO_2 concentrations. The HOM dimers are
748   formed earlier compared to under ambient conditions and then can go through the further
749   oxidation reactions. Note that this does not mean the maximum concentrations of HOM dimers
750   will also accurately occur at the same OH exposures in the atmosphere, because the detailed
751   appearance time of the maximum concentrations of HOM dimers is dependent on their
752   formation rate and loss rate. In our experiments, the formation rate and loss rate were not
753   accelerated equally. On the other hand, the loss pathways of HOM dimers were not exactly the
754   same as the ambient due to the lack of aerosols in the OFR. With the decrease of particulate
755   pollution and thus condensation sinks in the polluted areas, the physical loss of HOMs might
756   be lower and the chemical process can be more important. This series of experiments are not
757   meant to specifically find out the detailed OH exposures when the maximum concentrations of
758   HOM dimers will occur, but try to indicate how HOM dimers evolve with the increase of OH
759   exposures. This work can be regarded as an indicator for the potential chemical fates of HOM
760   dimers in the atmosphere if their survival time permitted. It should be noted that the gas-phase
761   chemistry in the PAM OFR cannot be exactly the same as that in the ambient. Reactions of OH
762   with OVOCs often lead to HO_2 formation, resulting in a $HO_2{:}RO_2$ ratio larger than 1 in the real

atmosphere (Bianchi et al., 2019). A recent campaign conducted at a rural site in the Yangtze River Delta estimated that the local ratio of HO_2:RO_2, the latter of which was presumably derived from longer chain alkanes ($> C_3$), alkenes, and aromatic compounds, was around 1.66 (Ma et al., 2022). Such a high HO_2:RO_2 ratio condition is typically difficult to be simulated in the laboratory experiments, as the precursors are usually hydrocarbons without any OVOCs (Peng and Jimenez, 2020). This is exactly the case for our experiments, but its influences on our conclusion were tiny, as have been discussed in the Section 3.1. Therefore, the difference in the distribution of products will not change our conclusion.

Such an active secondary OH chemistry is consistent with the fast OH reaction rates of HOMs. We take $C_{18}H_{26}O_8$ whose plausible structure is shown in Figure S4 as an example, which is the accretion product of two $C_9H_{13}O_5\cdot$. Its OH reaction rate constant is estimated to be around 2.07×10^{-10} cm^3 $molecule^{-1}$ s^{-1} according to the structure-activity relationship (Jenkin et al., 2018b, a), whose details are provided in Supplementary Text S2. This rate is several times larger than that of 1,3,5-TMB, which enables a very active secondary OH chemistry in the system. MCM recommended an OH reaction rate of 1.28×10^{-10} cm^3 $molecule^{-1}$ s^{-1} for TM135BPOOH ($C_9H_{14}O_5$) and 1.00×10^{-10} cm^3 $molecule^{-1}$ s^{-1} for TM135OBPOH ($C_9H_{12}O_4$) (Jenkin et al., 2003). The OH reaction rate for $C_{18}H_{26}O_8$ should also be fast due to the C=C bonds in its structure, which is activated by the adjacent functionalities. Our calculation result is consistent with this estimation.

The distributions of C18 organonitrates also verified the extensive secondary reactions. The most abundant C18 organonitrate, $C_{18}H_{27}NO_{12}$ was a NO termination product of radical $C_{18}H_{27}O_{11}\cdot$, which, as mentioned above, was the radical generated from the OH reaction with $C_{18}H_{26}O_8$. $C_{18}H_{27}NO_{12}$ can also be formed either by accretion between a $C_9H_{15}O_m\cdot$ radical and a $C_9H_{12}NO_m\cdot$ radical or accretion between a $C_9H_{13}O_m\cdot$ radical and a $C_9H_{14}NO_m\cdot$ radical. Both $C_9H_{15}O_m\cdot$ and $C_9H_{14}NO_m\cdot$ radicals are a typical multi-generation RO_2 and thus prove $C_{18}H_{27}NO_{12}$ is a multi-generation OH oxidation product. Other C18 organonitrates are believed to be formed in a similar pathway. Hence, plenty of organonitrates have been formed via the multi-generation OH reactions of first-generation stabilized products.

3.3 Oxidation products in low [OH] experiments

Given the larger sampling port, lower initial ozone concentrations, lower UV light intensities, and a better performance of mass spectrometer in this series of low [OH] experiments, a number of new species were detected in the 2nd-round experiments, including three typical termination reaction products of BPR, i.e., $C_9H_{14}O_4$, $C_9H_{14}O_5$, and $C_9H_{13}NO_6$, and a number of low volatile compounds, e.g., $C_9H_xO_{11}$ (x = 12 - 15). The distributions of oxidation products detected by nitrate CI-TOF in Exp. 2-3, 2-4, and 2-7, representative low [OH]

798 experiments, are displayed in Figure 5. The detailed molecular formula and their contributions
799 to total HOMs signals are provided in Tables S6 and S7.

800   In addition, certain C9 and C18 HOMs with lower DBE than typical first-generation
801 products predicted by MCM (Saunders et al., 2003) or reported by previous studies (Berndt et
802 al., 2018b), were detected in Exp. 2-3, 2-4, and 2-7, although [OH] in these experiments are
803 much lower than those in the 1st-round experiments.

804   Observation of compounds with lower DBE in Exp. 2-3, 2-4, and 2-7 including HOM
805 monomers with DBE lower than 3 and HOM dimers with DBE lower than 6, as well as
806 monomer radicals with DBE lower than 3 including $C_9H_{15}O_m\cdot$ (m = 7 - 11) and $C_9H_{14}NO_9\cdot$,
807 proves the re-initiation of OH oxidation of the stabilized products in experiments with
808 atmospheric relevant [OH]. All the stabilized products and radicals depicted in the proposed
809 mechanisms (Scheme 2 and Scheme 3) were detected in both Exp. 2-3 and Exp. 2-4, except for
810 $C_9H_{15}O_9\cdot$ that was only detected in Exp. 2-3. This means that the proposed reaction pathways
811 have already happened under atmospheric [OH] conditions with limited OH exposures.
812 However, as we do not know the exact structures of these OOMs and radicals, the proposed
813 reaction pathways are merely based on the chemical formulae detected by nitrate CIMS and
814 nitrate CI-TOF and proposed according to the general mechanisms of OH addition reactions to
815 the C=C bond. Other reaction pathways to generate these compounds or other isomers
816 generated in these pathways are undoubtedly feasible.

817   A lot of compounds detected in the experiments without NO_x were not observed in
818 counterpart experiments with NO_x. We also did not detect decent signals of HOM dimers in the
819 NO_x-present experiments in the 2nd-round experiments. This might come from the dominant
820 significance of $NO + RO_2$ reactions ($R8$ - $R9$) after the introduction of NO_x into system, making
821 signals of certain HOMs from other channels lower than the detection limit of the instrument.
822 The proportions of other reaction channels decreased, and were reassigned to the NO channel,
823 as evidenced by the fact that most of observed oxidation products were organonitrates, which
824 is in an excellent agreement with the modeled channel proportions in Section 3.1.

825   Many organonitrates were observed in both series of experiments. In the low [OH]
826 experiments, the most significant compound was $C_9H_{13}NO_8$, whose formula matches the NO
827 termination product of $C_9H_{13}O_7\cdot$, i.e., autoxidation product of BPR. The second most important
828 compound, $C_9H_{14}N_2O_{10}$ in our low [OH] experiments, was the most significant product in the
829 high [OH] experiments in presence of NO_x, whose formula matches the NO termination product
830 of $C_9H_{14}NO_9\cdot$, i.e., the RO_2 formed via an OH addition to $C_9H_{13}NO_6$, the NO termination
831 product of BPR. All of the products and radicals mentioned above were observed in Exp. 2-7,
832 as shown in Figure 5c. From the perspective of molecular formula, $C_9H_{14}N_2O_{10}$ is also one of

833 the most frequently observed multi-nitrogen-containing compound in polluted atmospheres,

834 whose seasonal variations show a good correlation with [OH] (Guo et al., 2022; Yang et al.,

835 2023).

836   A comparison of relative abundances of C9 and C18 products under different [OH] levels

837 is helpful for the elucidation of their formation pathways. The difference in product

838 distributions between Exp. 2-3 ([OH] = ~1.69×10^7 molecule cm^{-3}) and Exp. 2-1 ([OH] =

839 ~1.03×10^8 molecule cm^{-3}), as well as between Exp. 2-3 and Exp. 1-12 ([OH] = ~8.47×10^8

840 molecule cm^{-3}) is shown in Figure 6. The normalized abundance was obtained by normalizing

841 all the products to the most abundant one in each experiment, i.e., $C_{18}H_{26}O_{10}$ in Exp. 2-1 and

842 Exp. 2-3, and $C_9H_{14}O_7$ in Exp. 1-12. The changes in the normalized abundance were obtained

843 by subtracting the normalized abundance in Exp. 2-1 from that in Exp. 2-3, and Exp. 1-12 from

844 Exp. 2-3. As the [OH] and OH exposure increased, there was a noticeable rise in the relative

845 abundance of more oxygenated compounds, which can be attributed to the more intensive

846 proportion of multi-generation OH oxidation in high OH exposure experiments. This

847 comparison demonstrates the capacity and potential of multi-generation OH oxidation to reduce

848 DBE and elevate the oxygenated levels of oxidation products.

849   In conclusion, observation of the same low DBE compounds, i.e., DBE = 2, in both low

850 [OH] and high [OH] experiments confirms the feasibility of the generation of HOMs under

851 atmospheric relevant conditions. The detection of $C_9H_{14}O_5$, $C_9H_{15}O_8\cdot$, $C_9H_{14}O_7$, $C_9H_{14}O_8$,

852 $C_9H_{15}O_7\cdot$, and $C_9H_{16}O_8$, and $C_9H_{14}O_6$, $C_9H_{15}O_9\cdot$, $C_9H_{14}O_8$, $C_9H_{14}O_9$, $C_9H_{15}O_8\cdot$, and $C_9H_{16}O_9$, in

853 low [OH] experiments also confirms the potential existence of the proposed mechanisms, i.e.,

854 Scheme 2 and Scheme 3, respectively. Certainly, other potential formation pathways for these

855 products are possible.

856 **(a)**

857
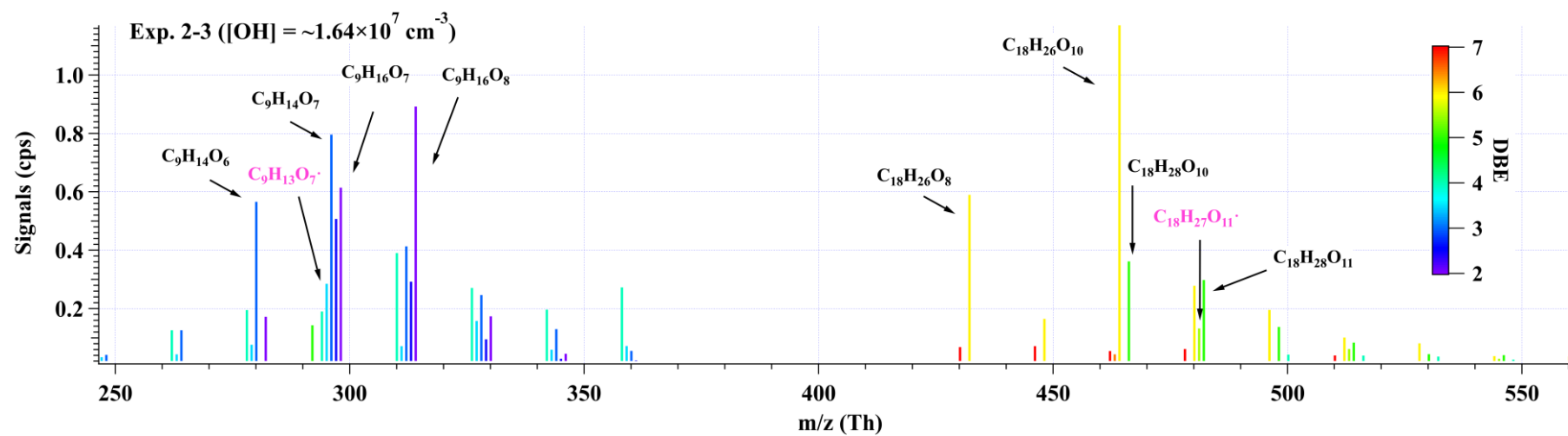
858 **(b)**
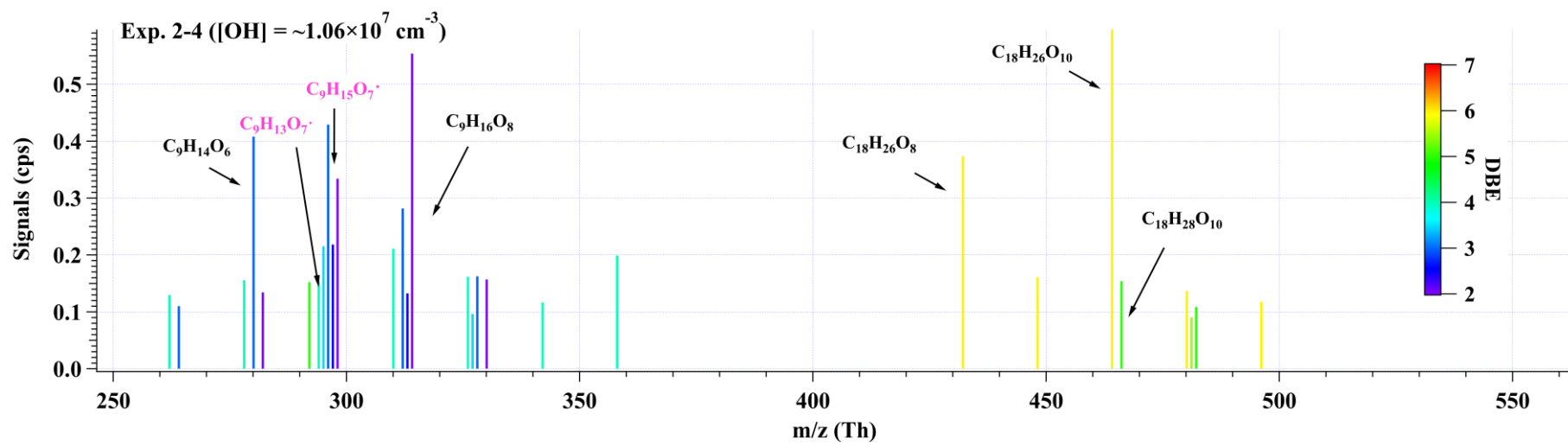
(c)
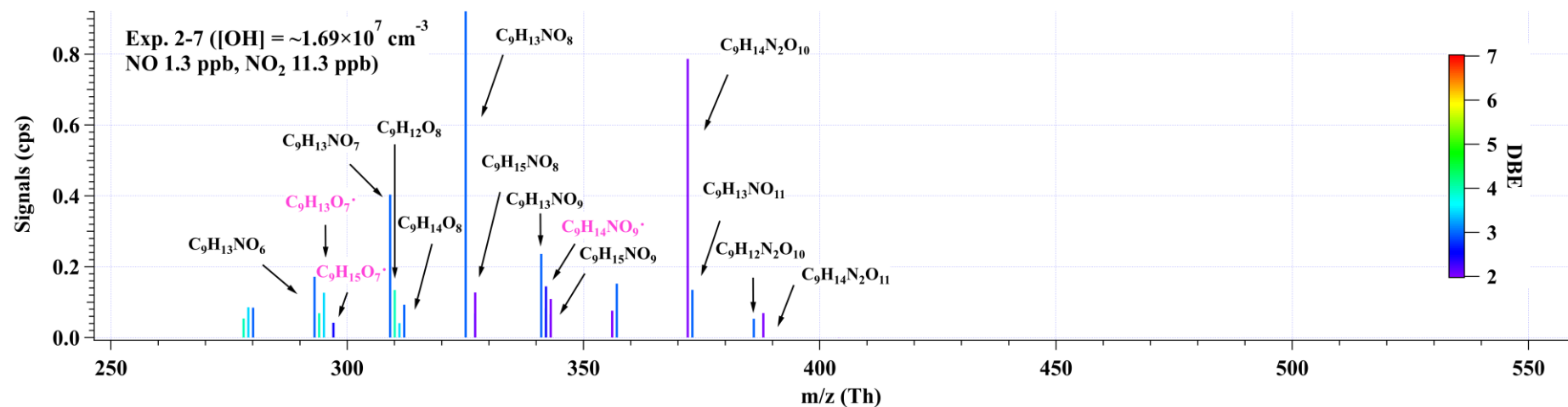
861

862

863 **Figure 5.** Distributions of C9 and C18 products detected by nitrate CI-TOF in (a) Exp. 2-3, (b) Exp. 2-4, and (c) Exp. 2-7. The reagent ion, NO_3^-, is omitted in

864 the label for the molecular formula. Important radicals were labelled in pink. Note that no convinced signals of HOM dimers were observed in the 2nd-round

865 experiments with NO_x.

866

(a)
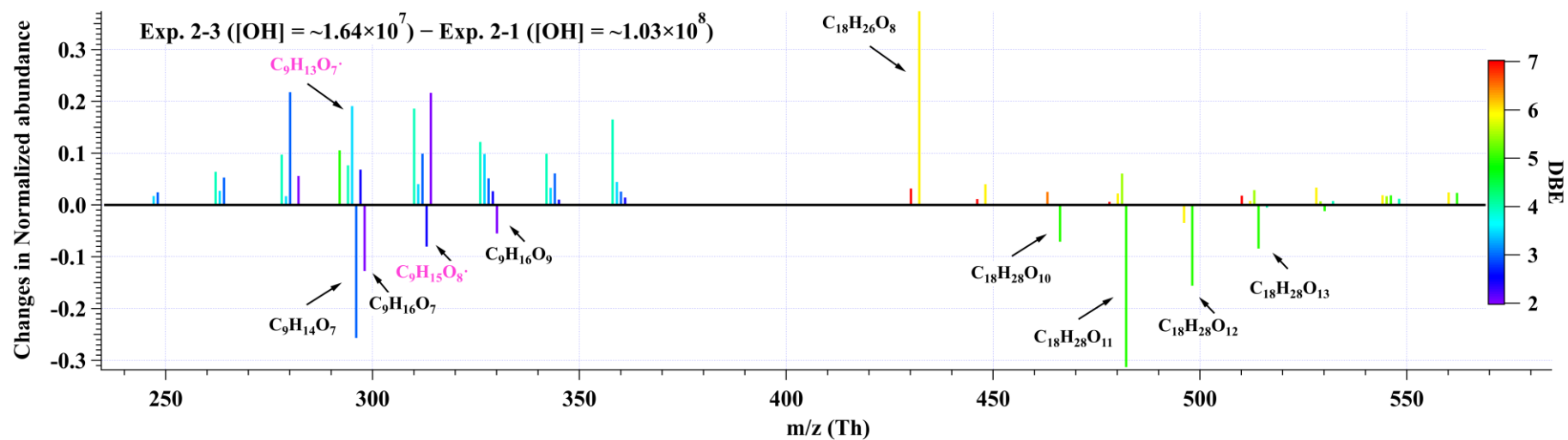
(b)
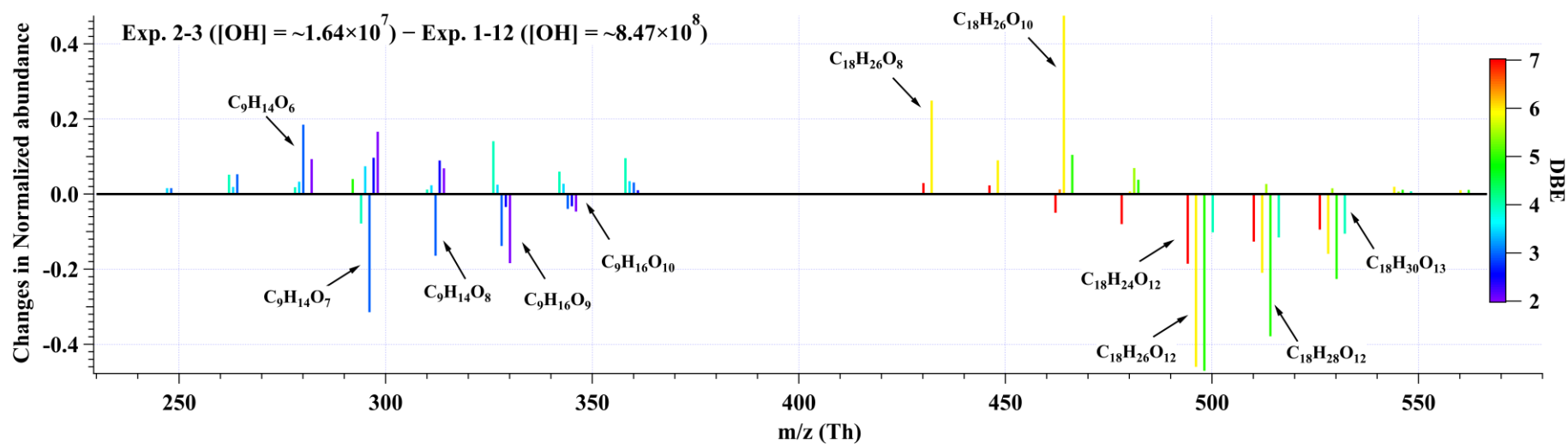
871

872 **Figure 6**. The changes in normalized abundance of C9 and C18 products observed by nitrate CI-TOF in (a) Exp.2-3 relative to Exp.2-1, and (b) Exp.2-3

873 relative to Exp.1-12. The reagent ion, NO_3^-, is omitted in the label. The normalized abundance was obtained by normalizing all the products to the most

874 abundant one in each experiment, i.e., $C_{18}H_{26}O_{10}$ in Exp.2-1 and Exp.2-3, and $C_9H_{14}O_7$ in Exp.1-12.

4 Atmospheric Implications

This study highlights the influences of OH exposure on the distribution and evolution of 1,3,5-TMB-derived HOMs. Secondary OH reactions can influence HOMs' composition by directly reacting with the stabilized first-generation oxidation products, leading to enhanced formation of HOMs, if the stabilized, first-generation oxidation products could survive from condensation loss onto pre-existing particles. Observation of organonitrates generated in the NO experiments further confirmed ~~this~~the secondary OH oxidation. Due to the elevated abundance and the reduced volatility of HOMs, growth rates of newly formed nanoparticles in the presence of HOMs ~~should~~could be raised, especially in high-OH environments, which prevails in the summer noon. Substantially high concentrations of OH have been frequently observed in polluted environments during summer, e.g., megacities in China (Tan et al., 2019), and thus more active secondary OH reactions are expected compared to wintertime. As a plausible consequence, seasonal differences of HOMs and new particle formation (NPF) are resulted (Qiao et al., 2021; Yao et al., 2018; Guo et al., 2022). Furthermore, previous studies suggest that high concentrations of NO can suppress the formation of HOMs via the suppression of autoxidation (Pye et al., 2019), but the influences of such a suppression could have been overestimated, since secondary OH reactions can continue to oxidize the stabilized organonitrates. Our conclusions help to explain the existing gap between model prediction and ambient measurement on the HOMs concentrations (Qi et al., 2018), and to build a global HOMs simulation model.

Data availability. Data used in this work are available upon request from the corresponding authors.

Supplement. The supplement related to this article is available online.

Author contributions. LW and Yuwei Wang designed the experiments. Yuwei Wang conducted the laboratory experiments. Yuwei Wang analyzed the data. Yuwei Wang and LW wrote the paper. All co-authors discussed the results and commented on the manuscript.

Competing interests. The authors declare that they have no conflict of interest.

Acknowledgments. This work was financially supported by the National Natural Science Foundation of China (21925601, 22127811). The authors declare no competing interests.

909   Yuwei Wang would like to thank Andrew T. Lambe, Peng Zhe, and Jose Jimenez for helpful

910   discussions on PAM experiments.

References

911 **References**

912 Berndt, T., Mentler, B., Scholz, W., Fischer, L., Herrmann, H., Kulmala, M., and Hansel, A.:
913 Accretion Product Formation from Ozonolysis and OH Radical Reaction of α-Pinene:
914 Mechanistic Insight and the Influence of Isoprene and Ethylene, Environ. Sci. Technol., 52,
915 11069–11077, https://doi.org/10.1021/acs.est.8b02210, 2018a.
916 Berndt, T., Scholz, W., Mentler, B., Fischer, L., Herrmann, H., Kulmala, M., and Hansel, A.:
917 Accretion Product Formation from Self- and Cross-Reactions of RO2 Radicals in the
918 Atmosphere, Angew. Chemie - Int. Ed., 57, 3820–3824,
919 https://doi.org/10.1002/anie.201710989, 2018b.
920 Bianchi, F., Kurtén, T., Riva, M., Mohr, C., Rissanen, M. P., Roldin, P., Berndt, T., Crounse,
921 J. D., Wennberg, P. O., Mentel, T. F., Wildt, J., Junninen, H., Jokinen, T., Kulmala, M.,
922 Worsnop, D. R., Thornton, J. A., Donahue, N., Kjaergaard, H. G., and Ehn, M.: Highly
923 Oxygenated Organic Molecules (HOM) from Gas-Phase Autoxidation Involving Peroxy
924 Radicals: A Key Contributor to Atmospheric Aerosol, Chem. Rev., 119, 3472–3509,
925 https://doi.org/10.1021/acs.chemrev.8b00395, 2019.
926 Cheng, X., Chen, Q., Li, Y. J., Zheng, Y., Liao, K., and Huang, G.: Highly Oxygenated
927 Organic Molecules Produced by the Oxidation of Benzene and Toluene in a Wide Range of
928 OH Exposure and NOx Conditions, Atmos. Chem. Phys., 1–23, https://doi.org/10.5194/acp-
929 2021-201, 2021.
930 Crounse, J. D., Nielsen, L. B., Jørgensen, S., Kjaergaard, H. G., and Wennberg, P. O.:
931 Autoxidation of organic compounds in the atmosphere, J. Phys. Chem. Lett., 4, 3513–3520,
932 https://doi.org/10.1021/jz4019207, 2013.
933 Deng, C., Fu, Y., Dada, L., Yan, C., Cai, R., Yang, D., Zhou, Y., Yin, R., Lu, Y., Li, X., Qiao,
934 X., Fan, X., Nie, W., Kontkanen, J., Kangasluoma, J., Chu, B., Ding, A., Kerminen, V. M.,
935 Paasonen, P., Worsnop, D. R., Bianchi, F., Liu, Y., Zheng, J., Wang, L., Kulmala, M., and
936 Jiang, J.: Seasonal characteristics of new particle formation and growth in urban Beijing,
937 Environ. Sci. Technol., 54, 8547–8557, https://doi.org/10.1021/acs.est.0c00808, 2020.
938 Ehn, M., Thornton, J. A., Kleist, E., Sipilä, M., Junninen, H., Pullinen, I., Springer, M.,
939 Rubach, F., Tillmann, R., Lee, B., Lopez-Hilfiker, F., Andres, S., Acir, I. H., Rissanen, M.,
940 Jokinen, T., Schobesberger, S., Kangasluoma, J., Kontkanen, J., Nieminen, T., Kurtén, T.,
941 Nielsen, L. B., Jørgensen, S., Kjaergaard, H. G., Canagaratna, M., Maso, M. D., Berndt, T.,
942 Petäjä, T., Wahner, A., Kerminen, V. M., Kulmala, M., Worsnop, D. R., Wildt, J., and
943 Mentel, T. F.: A large source of low-volatility secondary organic aerosol, Nature, 506, 476–
944 479, https://doi.org/10.1038/nature13032, 2014.
945 Eisele, F. L. and Tanner, D. J.: Measurement of the gas phase concentration of H 2 SO 4 and
946 methane sulfonic acid and estimates of H 2 SO 4 production and loss in the atmosphere, J.
947 Geophys. Res. Atmos., 98, 9001–9010, https://doi.org/10.1029/93JD00031, 1993.
948 Garmash, O., Rissanen, M. P., Pullinen, I., Schmitt, S., Kausiala, O., Tillmann, R., Zhao, D.,
949 Percival, C., Bannan, T. J., Priestley, M., Hallquist, Å. M., Kleist, E., Kiendler-Scharr, A.,
950 Hallquist, M., Berndt, T., McFiggans, G., Wildt, J., Mentel, T. F., and Ehn, M.: Multi-
951 generation OH oxidation as a source for highly oxygenated organic molecules from
952 aromatics, Atmos. Chem. Phys., 20, 515–537, https://doi.org/10.5194/acp-20-515-2020, 2020.

953 Guo, Y., Yan, C., Liu, Y., Qiao, X., Zheng, F., Zhang, Y., Zhou, Y., Li, C., Fan, X., Lin, Z.,
954 Feng, Z., Zhang, Y., Zheng, P., Tian, L., Nie, W., Wang, Z., Huang, D., Daellenbach, K. R.,
955 Yao, L., Dada, L., Bianchi, F., Jiang, J., Liu, Y., Kerminen, V. M., and Kulmala, M.: Seasonal
956 variation in oxygenated organic molecules in urban Beijing and their contribution to
957 secondary organic aerosol, Atmos. Chem. Phys., 22, 10077–10097,
958 https://doi.org/10.5194/acp-22-10077-2022, 2022.

959 Heinritzi, M., Simon, M., Steiner, G., Wagner, A. C., Kürten, A., Hansel, A., and Curtius, J.:
960 Characterization of the mass-dependent transmission efficiency of a CIMS, Atmos. Meas.
961 Tech., 9, 1449–1460, https://doi.org/10.5194/amt-9-1449-2016, 2016.

962 Hyttinen, N., Kupiainen-Määttä, O., Rissanen, M. P., Muuronen, M., Ehn, M., and Kurtén, T.:
963 Modeling the Charging of Highly Oxidized Cyclohexene Ozonolysis Products Using Nitrate-
964 Based Chemical Ionization, J. Phys. Chem. A, 119, 6339–6345,
965 https://doi.org/10.1021/acs.jpca.5b01818, 2015.

966 Iyer, S., Kumar, A., Savolainen, A., Barua, S., Daub, C., Pichelstorfer, L., Roldin, P.,
967 Garmash, O., Seal, P., Kurtén, T., and Rissanen, M.: Molecular rearrangement of bicyclic
968 peroxy radicals is a key route to aerosol from aromatics, Nat. Commun., 14, 4984,
969 https://doi.org/10.1038/s41467-023-40675-2, 2023.

970 Jacob, D. J.: Introduction to atmospheric chemistry, Princeton, 1999.

971 Jenkin, M. E., Saunders, S. M., Wagner, V., and Pilling, M. J.: Protocol for the development
972 of the Master Chemical Mechanism, MCM v3 (Part B): tropospheric degradation of aromatic
973 volatile organic compounds, Atmos. Chem. Phys., 3, 181–193, https://doi.org/10.5194/acp-3-
974 181-2003, 2003.

975 Jenkin, M. E., Valorso, R., Aumont, B., Rickard, A. R., and Wallington, T. J.: Estimation of
976 rate coefficients and branching ratios for gas-phase reactions of OH with aliphatic organic
977 compounds for use in automated mechanism construction, 9297–9328 pp.,
978 https://doi.org/10.5194/acp-18-9297-2018, 2018a.

979 Jenkin, M. E., Valorso, R., Aumont, B., Rickard, A. R., and Wallington, T. J.: Estimation of
980 rate coefficients and branching ratios for gas-phase reactions of OH with aromatic organic
981 compounds for use in automated mechanism construction, Atmos. Chem. Phys., 18, 9329–
982 9349, https://doi.org/10.5194/acp-18-9329-2018, 2018b.

983 Keller-Rudek, H., Moortgat, G. K., Sander, R., and Sörensen, R.: The MPI-Mainz UV/VIS
984 spectral atlas of gaseous molecules of atmospheric interest, Earth Syst. Sci. Data, 5, 365–373,
985 https://doi.org/10.5194/essd-5-365-2013, 2013.

986 Krechmer, J., Lopez-Hilfiker, F., Koss, A., Hutterli, M., Stoermer, C., Deming, B., Kimmel,
987 J., Warneke, C., Holzinger, R., Jayne, J., Worsnop, D., Fuhrer, K., Gonin, M., and De Gouw,
988 J.: Evaluation of a New Reagent-Ion Source and Focusing Ion− Molecule Reactor for Use in
989 Proton-Transfer-Reaction Mass Spectrometry, Anal. Chem., 90, 12011–12018,
990 https://doi.org/10.1021/acs.analchem.8b02641, 2018.

991 Lambe, A., Massoli, P., Zhang, X., Canagaratna, M., Nowak, J., Daube, C., Yan, C., Nie, W.,
992 Onasch, T., Jayne, J., Kolb, C., Davidovits, P., Worsnop, D., and Brune, W.: Controlled nitric
993 oxide production via O(1D) + N2O reactions for use in oxidation flow reactor studies, Atmos.
994 Meas. Tech., 10, 2283–2298, https://doi.org/10.5194/amt-10-2283-2017, 2017.

995 Lambe, A., Krechmer, J., Peng, Z., Casar, J., Carrasquillo, A., Raff, J., Jimenez, J., and
996 Worsnop, D.: HO x and NO x production in oxidation flow reactors via photolysis of, 1–22,
997 2018.
998 Lambe, A. T., Ahern, A. T., Williams, L. R., Slowik, J. G., Wong, J. P. S., Abbatt, J. P. D.,
999 Brune, W. H., Ng, N. L., Wright, J. P., Croasdale, D. R., Worsnop, D. R., Davidovits, P., and
1000 Onasch, T. B.: Characterization of aerosol photooxidation flow reactors: heterogeneous
1001 oxidation, secondary organic aerosol formation and cloud condensation nuclei activity
1002 measurements, Atmos. Meas. Tech, 4, 445–461, https://doi.org/10.5194/amt-4-445-2011,
1003 2011.
1004 Lambe, A. T., Chhabra, P. S., Onasch, T. B., Brune, W. H., Hunter, J. F., Kroll, J. H.,
1005 Cummings, M. J., Brogan, J. F., Parmar, Y., Worsnop, D. R., Kolb, C. E., and Davidovits, P.:
1006 Effect of oxidant concentration, exposure time, and seed particles on secondary organic
1007 aerosol chemical composition and yield, Atmos. Chem. Phys., 15, 3063–3075,
1008 https://doi.org/10.5194/acp-15-3063-2015, 2015.
1009 Lehtipalo, K., Yan, C., Dada, L., Bianchi, F., Xiao, M., Wagner, R., Stolzenburg, D., Ahonen,
1010 L. R., Amorim, A., Baccarini, A., Bauer, P. S., Baumgartner, B., Bergen, A., Bernhammer, A.
1011 K., Breitenlechner, M., Brilke, S., Buchholz, A., Mazon, S. B., Chen, D., Chen, X., Dias, A.,
1012 Dommen, J., Draper, D. C., Duplissy, J., Ehn, M., Finkenzeller, H., Fischer, L., Frege, C.,
1013 Fuchs, C., Garmash, O., Gordon, H., Hakala, J., He, X., Heikkinen, L., Heinritzi, M., Helm, J.
1014 C., Hofbauer, V., Hoyle, C. R., Jokinen, T., Kangasluoma, J., Kerminen, V. M., Kim, C.,
1015 Kirkby, J., Kontkanen, J., Kürten, A., Lawler, M. J., Mai, H., Mathot, S., Mauldin, R. L.,
1016 Molteni, U., Nichman, L., Nie, W., Nieminen, T., Ojdanic, A., Onnela, A., Passananti, M.,
1017 Petäjä, T., Piel, F., Pospisilova, V., Quéléver, L. L. J., Rissanen, M. P., Rose, C., Sarnela, N.,
1018 Schallhart, S., Schuchmann, S., Sengupta, K., Simon, M., Sipilä, M., Tauber, C., Tomé, A.,
1019 Tröstl, J., Väisänen, O., Vogel, A. L., Volkamer, R., Wagner, A. C., Wang, M., Weitz, L.,
1020 Wimmer, D., Ye, P., Ylisirniö, A., Zha, Q., Carslaw, K. S., Curtius, J., Donahue, N. M.,
1021 Flagan, R. C., Hansel, A., Riipinen, I., Virtanen, A., Winkler, P. M., Baltensperger, U.,
1022 Kulmala, M., and Worsnop, D. R.: Multicomponent new particle formation from sulfuric
1023 acid, ammonia, and biogenic vapors, Sci. Adv., 4, 1–10,
1024 https://doi.org/10.1126/sciadv.aau5363, 2018.
1025 Li, R., Palm, B. B., Ortega, A. M., Hlywiak, J., Hu, W., Peng, Z., Day, D. A., Knote, C.,
1026 Brune, W. H., De Gouw, J. A., and Jimenez, J. L.: Modeling the radical chemistry in an
1027 oxidation flow reactor: Radical formation and recycling, sensitivities, and the OH exposure
1028 estimation equation, J. Phys. Chem. A, 119, 4418–4432, https://doi.org/10.1021/jp509534k,
1029 2015.
1030 Lu, K. D., Rohrer, F., Holland, F., Fuchs, H., Bohn, B., Brauers, T., Chang, C. C., Häseler, R.,
1031 Hu, M., Kita, K., Kondo, Y., Li, X., Lou, S. R., Nehr, S., Shao, M., Zeng, L. M., Wahner, A.,
1032 Zhang, Y. H., and Hofzumahaus, A.: Observation and modelling of OH and HO2
1033 concentrations in the Pearl River Delta 2006: A missing OH source in a VOC rich
1034 atmosphere, Atmos. Chem. Phys., 12, 1541–1569, https://doi.org/10.5194/acp-12-1541-2012,
1035 2012.
1036 Ma, X., Tan, Z., Lu, K., Yang, X., Chen, X., Wang, H., Chen, S., Fang, X., Li, S., Li, X., Liu,
1037 J., Liu, Y., Lou, S., Qiu, W., Wang, H., Zeng, L., and Zhang, Y.: OH and HO2 radical

chemistry at a suburban site during the EXPLORE-YRD campaign in 2018, Atmos. Chem. Phys., 22, 7005–7028, https://doi.org/10.5194/acp-22-7005-2022, 2022.

Mehra, A., Wang, Y., E. Krechmer, J., Lambe, A., Majluf, F., A. Morris, M., Priestley, M., J. Bannan, T., J. Bryant, D., L. Pereira, K., F. Hamilton, J., R. Rickard, A., J. Newland, M., Stark, H., Croteau, P., T. Jayne, J., R. Worsnop, D., R. Canagaratna, M., Wang, L., and Coe, H.: Evaluation of the chemical composition of gas- And particle-phase products of aromatic oxidation, Atmos. Chem. Phys., 20, 9783–9803, https://doi.org/10.5194/acp-20-9783-2020, 2020.

Mentel, T. F., Springer, M., Ehn, M., Kleist, E., Pullinen, I., Kurtén, T., Rissanen, M., Wahner, A., and Wildt, J.: Formation of highly oxidized multifunctional compounds: Autoxidation of peroxy radicals formed in the ozonolysis of alkenes - Deduced from structure-product relationships, Atmos. Chem. Phys., 15, 6745–6765, https://doi.org/10.5194/acp-15-6745-2015, 2015.

Mohr, C., Thornton, J. A., Heitto, A., Lopez-hil, F. D., Lutz, A., Riipinen, I., Hong, J., Donahue, N. M., Hallquist, M., Petäjä, T., Kulmala, M., and Yli-juuti, T.: Molecular identification of organic vapors driving atmospheric nanoparticle growth, Nat. Commun., 1–7, https://doi.org/10.1038/s41467-019-12473-2, 2019.

Molteni, U., Bianchi, F., Klein, F., Haddad, I. El, Frege, C., Rossi, M. J., Dommen, J., and Baltensperger, U.: Formation of highly oxygenated organic molecules from aromatic compounds, Atmos. Chem. Phys, 18, 1909–1921, https://doi.org/10.5194/acp-18-1909-2018, 2018.

Ng, N. L., Canagaratna, M. R., Zhang, Q., Jimenez, J. L., Tian, J., Ulbrich, I. M., Kroll, J. H., Docherty, K. S., Chhabra, P. S., Bahreini, R., Murphy, S. M., Seinfeld, J. H., Hildebrandt, L., Donahue, N. M., Decarlo, P. F., Lanz, V. A., Prévôt, A. S. H., Dinar, E., Rudich, Y., and Worsnop, D. R.: Organic aerosol components observed in Northern Hemispheric datasets from Aerosol Mass Spectrometry, Atmos. Chem. Phys., 10, 4625–4641, https://doi.org/10.5194/acp-10-4625-2010, 2010.

Orlando, J. J. and Tyndall, G. S.: Laboratory studies of organic peroxy radical chemistry: An overview with emphasis on recent issues of atmospheric significance, Chem. Soc. Rev., 41, 6294–6317, https://doi.org/10.1039/c2cs35166h, 2012.

Otkjær, R. V., Jakobsen, H. H., Tram, C. M., and Kjaergaard, H. G.: Calculated Hydrogen Shift Rate Constants in Substituted Alkyl Peroxy Radicals, J. Phys. Chem. A, 122, 8665–8673, https://doi.org/10.1021/acs.jpca.8b06223, 2018.

Peng, Z. and Jimenez, J. L.: Radical chemistry in oxidation flow reactors for atmospheric chemistry research, Chem. Soc. Rev., 49, 2570–2616, https://doi.org/10.1039/c9cs00766k, 2020.

Peng, Z., Day, D. A., Ortega, A. M., Palm, B. B., Hu, W., Stark, H., Li, R., Tsigaridis, K., Brune, W. H., and Jimenez, J. L.: Non-OH chemistry in oxidation flow reactors for the study of atmospheric chemistry systematically examined by modeling, Atmos. Chem. Phys., 16, 4283–4305, https://doi.org/10.5194/acp-16-4283-2016, 2016.

Pye, H. O. T., D'Ambro, E. L., Lee, B. H., Schobesberger, S., Takeuchi, M., Zhao, Y., Lopez-Hilfiker, F., Liu, J., Shilling, J. E., Xing, J., Mathur, R., Middlebrook, A. M., Liao, J., Welti, A., Graus, M., Warneke, C., de Gouw, J. A., Holloway, J. S., Ryerson, T. B., Pollack, I. B., and Thornton, J. A.: Anthropogenic enhancements to production of highly oxygenated

molecules from autoxidation, Proc. Natl. Acad. Sci. U. S. A., 116, 6641–6646,
https://doi.org/10.1073/pnas.1810774116, 2019.

Qi, X., Ding, A., Roldin, P., Xu, Z., Zhou, P., Sarnela, N., Nie, W., Huang, X., Rusanen, A.,
Ehn, M., Rissanen, M. P., Petäjä, T., Kulmala, M., and Boy, M.: Modelling studies of HOMs
and their contributions to new particle formation and growth: comparison of boreal forest in
Finland and a polluted environment in China, Atmos. Chem. Phys, 18, 11779–11791,
https://doi.org/10.5194/acp-18-11779-2018, 2018.

Qiao, X., Yan, C., Li, X., Guo, Y., Yin, R., Deng, C., Li, C., Nie, W., Wang, M., Cai, R.,
Huang, D., Wang, Z., Yao, L., Worsnop, D. R., Bianchi, F., Liu, Y., Donahue, N. M.,
Kulmala, M., and Jiang, J.: Contribution of Atmospheric Oxygenated Organic Compounds to
Particle Growth in an Urban Environment, Environ. Sci. Technol.,
https://doi.org/10.1021/acs.est.1c02095, 2021.

Qu, H., Wang, Y., Zhang, R., Liu, X., Huey, L. G., Sjostedt, S., Zeng, L., Lu, K., Wu, Y.,
Shao, M., Hu, M., Tan, Z., Fuchs, H., Broch, S., Wahner, A., Zhu, T., and Zhang, Y.:
Chemical Production of Oxygenated Volatile Organic Compounds Strongly Enhances
Boundary-Layer Oxidation Chemistry and Ozone Production, Environ. Sci. Technol., 55,
13718–13727, https://doi.org/10.1021/acs.est.1c04489, 2021.

Saunders, S. M., Jenkin, M. E., Derwent, R. G., and Pilling, M. J.: Protocol for the
development of the Master Chemical Mechanism, MCM v3 (Part A): Tropospheric
degradation of non-aromatic volatile organic compounds, Atmos. Chem. Phys., 3, 161–180,
https://doi.org/10.5194/acp-3-161-2003, 2003.

Stolzenburg, D., Fischer, L., Vogel, A. L., Heinritzi, M., Schervish, M., Simon, M., Wagner,
A. C., Dada, L., Ahonen, L. R., Amorim, A., Baccarini, A., Bauer, P. S., Baumgartner, B.,
Bergen, A., Bianchi, F., Breitenlechner, M., Brilke, S., Mazon, S. B., Chen, D., Dias, A.,
Draper, D. C., Duplissy, J., Haddad, I. El, Finkenzeller, H., Frege, C., Fuchs, C., Garmash, O.,
Gordon, H., He, X., Helm, J., Hofbauer, V., Hoyle, C. R., Kim, C., Kirkby, J., Kontkanen, J.,
Kürten, A., Lampilahti, J., Lawler, M., Lehtipalo, K., Leiminger, M., Mai, H., Mathot, S.,
Mentler, B., Molteni, U., Nie, W., Nieminen, T., Nowak, J. B., Ojdanic, A., Onnela, A.,
Passananti, M., Petäjä, T., Quéléver, L. L. J., Rissanen, M. P., Sarnela, N., Schallhart, S.,
Tauber, C., Tomé, A., Wagner, R., Wang, M., Weitz, L., Wimmer, D., Xiao, M., Yan, C., Ye,
P., Zha, Q., Baltensperger, U., Curtius, J., Dommen, J., Flagan, R. C., Kulmala, M., Smith, J.
N., Worsnop, D. R., Hansel, A., Donahue, N. M., and Winkler, P. M.: Rapid growth of
organic aerosol nanoparticles over a wide tropospheric temperature range, Proc. Natl. Acad.
Sci. U. S. A., 115, 9122–9127, https://doi.org/10.1073/pnas.1807604115, 2018.

Tan, Z., Fuchs, H., Lu, K., Hofzumahaus, A., Bohn, B., Broch, S., Dong, H., Gomm, S.,
Häseler, R., He, L., Holland, F., Li, X., Liu, Y., Lu, S., Rohrer, F., Shao, M., Wang, B.,
Wang, M., Wu, Y., Zeng, L., Zhang, Y., Wahner, A., and Zhang, Y.: Radical chemistry at a
rural site (Wangdu) in the North China Plain: Observation and model calculations of OH,
HO2 and RO2 radicals, Atmos. Chem. Phys., 17, 663–690, https://doi.org/10.5194/acp-17-
663-2017, 2017.

Tan, Z., Rohrer, F., Lu, K., Ma, X., Bohn, B., Broch, S., Dong, H., Fuchs, H., Gkatzelis, G. I.,
Hofzumahaus, A., Holland, F., Li, X., Liu, Y., Liu, Y., Novelli, A., Shao, M., Wang, H., Wu,
Y., Zeng, L., Hu, M., Kiendler-Scharr, A., Wahner, A., and Zhang, Y.: Wintertime
photochemistry in Beijing: Observations of ROx radical concentrations in the North China

1126 Plain during the BEST-ONE campaign, Atmos. Chem. Phys., https://doi.org/10.5194/acp-18-
1127 12391-2018, 2018.

1128 Tan, Z., Lu, K., Jiang, M., Su, R., Wang, H., Lou, S., Fu, Q., Zhai, C., Tan, Q., Yue, D.,
1129 Chen, D., Wang, Z., Xie, S., Zeng, L., and Zhang, Y.: Daytime atmospheric oxidation
1130 capacity in four Chinese megacities during the photochemically polluted season: A case study
1131 based on box model simulation, Atmos. Chem. Phys., 19, 3493–3513,
1132 https://doi.org/10.5194/acp-19-3493-2019, 2019.

1133 Tröstl, J., Chuang, W. K., Gordon, H., Heinritzi, M., Yan, C., Molteni, U., Ahlm, L., Frege,
1134 C., Bianchi, F., Wagner, R., Simon, M., Lehtipalo, K., Williamson, C., Craven, J. S.,
1135 Duplissy, J., Adamov, A., Almeida, J., Bernhammer, A. K., Breitenlechner, M., Brilke, S.,
1136 Dias, A., Ehrhart, S., Flagan, R. C., Franchin, A., Fuchs, C., Guida, R., Gysel, M., Hansel, A.,
1137 Hoyle, C. R., Jokinen, T., Junninen, H., Kangasluoma, J., Keskinen, H., Kim, J., Krapf, M.,
1138 Kürten, A., Laaksonen, A., Lawler, M., Leiminger, M., Mathot, S., Möhler, O., Nieminen, T.,
1139 Onnela, A., Petäjä, T., Piel, F. M., Miettinen, P., Rissanen, M. P., Rondo, L., Sarnela, N.,
1140 Schobesberger, S., Sengupta, K., Sipilä, M., Smith, J. N., Steiner, G., Tomè, A., Virtanen, A.,
1141 Wagner, A. C., Weingartner, E., Wimmer, D., Winkler, P. M., Ye, P., Carslaw, K. S., Curtius,
1142 J., Dommen, J., Kirkby, J., Kulmala, M., Riipinen, I., Worsnop, D. R., Donahue, N. M., and
1143 Baltensperger, U.: The role of low-volatility organic compounds in initial particle growth in
1144 the atmosphere, Nature, 533, 527–531, https://doi.org/10.1038/nature18271, 2016.

1145 Tsiligiannis, E., Hammes, J., Salvador, C. M., Mentel, T. F., and Hallquist, M.: Effect of NOx
1146 on 1,3,5-trimethylbenzene (TMB) oxidation product distribution and particle formation,
1147 Atmos. Chem. Phys., 19, 15073–15086, https://doi.org/10.5194/acp-19-15073-2019, 2019.

1148 Vereecken, L.: Reaction Mechanisms for the Atmospheric Oxidation of Monocyclic Aromatic
1149 Compounds, Adv. Atmos. Chem., 377–527, https://doi.org/10.1142/9789813271838_0006,
1150 2019.

1151 Wang, M., Chen, D., Xiao, M., Ye, Q., Stolzenburg, D., Hofbauer, V., Ye, P., Vogel, A. L.,
1152 Mauldin, R. L., Amorim, A., Baccarini, A., Baumgartner, B., Brilke, S., Dada, L., Dias, A.,
1153 Duplissy, J., Finkenzeller, H., Garmash, O., He, X. C., Hoyle, C. R., Kim, C., Kvashnin, A.,
1154 Lehtipalo, K., Fischer, L., Molteni, U., Petäjä, T., Pospisilova, V., Quéléver, L. L. J.,
1155 Rissanen, M., Simon, M., Tauber, C., Tomé, A., Wagner, A. C., Weitz, L., Volkamer, R.,
1156 Winkler, P. M., Kirkby, J., Worsnop, D. R., Kulmala, M., Baltensperger, U., Dommen, J., El-
1157 Haddad, I., and Donahue, N. M.: Photo-oxidation of Aromatic Hydrocarbons Produces Low-
1158 Volatility Organic Compounds, Environ. Sci. Technol., 54, 7911–7921,
1159 https://doi.org/10.1021/acs.est.0c02100, 2020a.

1160 Wang, S., Wu, R., Berndt, T., Ehn, M., and Wang, L.: Formation of Highly Oxidized Radicals
1161 and Multifunctional Products from the Atmospheric Oxidation of Alkylbenzenes, Environ.
1162 Sci. Technol., 51, 8442–8449, https://doi.org/10.1021/acs.est.7b02374, 2017.

1163 Wang, W., Yuan, B., Peng, Y., Su, H., Cheng, Y., and Yang, S.: Direct observations indicate
1164 photodegradable oxygenated VOCs as larger contributors to radicals and ozone production in
1165 the atmosphere, Atmos. Chem. Phys., 1–28, 2022.

1166 Wang, Y., Mehra, A., Krechmer, J. E., Yang, G., Hu, X., Lu, Y., Lambe, A., Canagaratna, M.,
1167 Chen, J., Worsnop, D., Coe, H., and Wang, L.: Oxygenated products formed from OH-
1168 initiated reactions of trimethylbenzene: autoxidation and accretion, Atmos. Chem. Phys., 20,
1169 9563–9579, https://doi.org/10.5194/acp-20-9563-2020, 2020b.

Whalley, L. K., Slater, E. J., Woodward-Massey, R., Ye, C., Lee, J. D., Squires, F., Hopkins, J. R., Dunmore, R. E., Shaw, M., Hamilton, J. F., Lewis, A. C., Mehra, A., Worrall, S. D., Bacak, A., Bannan, T. J., Coe, H., Percival, C. J., Ouyang, B., Jones, R. L., Crilley, L. R., Kramer, L. J., Bloss, W. J., Vu, T., Kotthaus, S., Grimmond, S., Sun, Y., Xu, W., Yue, S., Ren, L., Joe, W., Nicholas Hewitt, C., Wang, X., Fu, P., and Heard, D. E.: Evaluating the sensitivity of radical chemistry and ozone formation to ambient VOCs and NOx in Beijing, Atmos. Chem. Phys., 21, 2125–2147, https://doi.org/10.5194/acp-21-2125-2021, 2021.

Xu, L., Møller, K. H., Crounse, J. D., Kjaergaard, H. G., and Wennberg, P. O.: New insights into the radical chemistry and product distribution in the OH-initiated oxidation of benzene, Environ. Sci. Technol., 54, 13467–13477, https://doi.org/10.1021/acs.est.0c04780, 2020.

Yang, C., Yao, N., Xu, L., Chen, G., Wang, Y., Fan, X., Zhou, P., Clusius, P., Tham, Y. J., Lin, Z., Chen, Y., Li, M., Hong, Y., and Chen, J.: Molecular Composition of Anthropogenic Oxygenated Organic Molecules and Their Contribution to Organic Aerosol in a Coastal City, Environ. Sci. Technol., 57, 15956–15967, https://doi.org/10.1021/acs.est.3c03244, 2023.

Yao, L., Garmash, O., Bianchi, F., Zheng, J., Yan, C., Kontkanen, J., Junninen, H., Mazon, S. B., Ehn, M., Paasonen, P., Sipilä, M., Wang, M., Wang, X., Xiao, S., Chen, H., Lu, Y., Zhang, B., Wang, D., Fu, Q., Geng, F., Li, L., Wang, H., Qiao, L., Yang, X., Chen, J., Kerminen, V.-M., Petäjä, T., Worsnop, D. R., Kulmala, M., and Wang, L.: Atmospheric new particle formation from sulfuric acid and amines in a Chinese megacity, Science (80-.)., 361, 278–281, https://doi.org/10.1126/science.aao4839, 2018.

Yuan, B., Chen, W., Shao, M., Wang, M., Lu, S., Wang, B., Liu, Y., Chang, C. C., and Wang, B.: Measurements of ambient hydrocarbons and carbonyls in the Pearl River Delta (PRD), China, Atmos. Res., 116, 93–104, https://doi.org/10.1016/j.atmosres.2012.03.006, 2012.

Zaytsev, A., Koss, A. R., Breitenlechner, M., Krechmer, J. E., Nihill, K. J., Lim, C. Y., Rowe, J. C., Cox, J. L., Moss, J., Roscioli, J. R., Canagaratna, M. R., Worsnop, D. R., Kroll, J. H., and Keutsch, F. N.: Mechanistic study of the formation of ring-retaining and ring-opening products from the oxidation of aromatic compounds under urban atmospheric conditions, Atmos. Chem. Phys., 19, 15117–15129, https://doi.org/10.5194/acp-19-15117-2019, 2019.

Zhao, Y., Thornton, J. A., and Pye, H. O. T.: Quantitative constraints on autoxidation and dimer formation from direct probing of monoterpene-derived peroxy radical chemistry, Proc. Natl. Acad. Sci., 115, 12142–12147, https://doi.org/10.1073/pnas.1812147115, 2018.